HBV

HØGSKOLEN I BUSKERUD OG VESTFOLD · PROFESJONSHØGSKOLEN ·

FACULTY OF TECHNOLOGY
AND MARITIME SCIENCES

Integratable Opto-Microfluidic Devices for Sensitive Detection of Bio-analytes

Doctoral Thesis

Nuno Miguel Matos Pires

2014

FACULTY OF TECHNOLOGY AND MARITIME SCIENCES

Integratable Opto-Microfluidic Devices for Sensitive Detection of Bio-analytes

Thesis submitted for the degree of Philosophiae Doctor

Nuno Miguel Matos Pires

Department of Micro- and Nanosystem Technology (IMST)
Faculty of Technology and Maritime Sciences (TekMar)
Buskerud and Vestfold University College (HBV)
Horten, 2014

Integratable Opto-Microfluidic Devices for Sensitive Detection of Bio-analytes

Department of Micro- and Nanosystem Technology (IMST)
Faculty of Technology and Maritime Sciences (TekMar)
Buskerud and Vestfold University College (HBV)
Horten, 2014

Doctoral theses at Buskerud and Vestfold University College, no. 3

ISSN: 1894-6380 (print)
ISSN: 1894-7530 (online)
ISBN: 978-82-7860-247-8 (print)
ISBN: 978-82-7860-248-5 (online)

Cover: HBV, Kommunikasjonsseksjonen
Printed at LOS digital

Abstract

The expensive fabrication of current optical microfluidic devices is a barrier to the successful implementation of these devices in low-cost, high-sensitivity biosensing systems. Organic photodiodes (OPDs) have great potential for application as photodetectors in integrated microfluidic devices due to their uncomplicated optical alignment, thin device architecture, precise control of the active area and simple device fabrication onto glass or polymer substrates. Recent developments in OPDs have resulted in new photoactive materials, such as poly[N-9′-heptadecanyl-2,7-carbazole-alt-5,5-(4′,7′-di-2-thienyl-2′,1′,3′-benzothiadiazole)] (PCDTBT), that have improved detectivity and stability. These unique optoelectronic characteristics enhance the detection sensitivity of OPD-integrated microfluidic biosensors while maintaining simple, inexpensive device fabrication.

To realise point-of-care (POC) detection of bio-analytes, the complexity of optical instrumentation must be minimised. Chemiluminescence (CL) offers an attractive solution to microfluidic analyte detection because it precludes the use of excitation light sources and emission filters. However, the low intensity of light emitted from CL reactions demands the use of highly sensitive photodetectors. Therefore, investigations of strategies to enhance CL assays and the combination of CL with PCDTBT-based detectors are the motivating factors for this work. Additionally, the enrichment of target organisms using a high-efficiency recovery method provides a route to optically detect bio-analytes at concentrations as low as hundreds or tens of organisms in a sample.

This doctoral thesis focuses on the following challenges: (i) demonstrate sensitive CL detection using a PCDTBT-based photodetector, (ii) investigate the integration of multiple OPDs in high-throughput microfluidic chips to realise multiplexed CL detection and (iii) explore methods for enhancing the sensitivity of opto-microfluidic detection. The progress made towards addressing these challenges is summarised below.

Article I reported the design and fabrication of an integrated optical microfluidic device employing a PCDTBT-based photodetector. The response of the OPD to CL light was enhanced by optimising the thickness of the photoactive layer and the hole transport layer. The current-voltage response due to detection of a medically relevant protein analyte was characterised. Further demonstration of quantitative CL detection with the optimised OPD was conducted in *Article II*. The opto-microfluidic device was found to

exhibit a linear response over four orders of magnitude, with a detection limit of approximately tens of picograms per millilitre and a detection sensitivity of approximately hundreds of picograms per millilitre. Moreover, high reproducibility and specificity to CL detection was observed, indicating the capability of the integrated OPD for POC applications.

Article III developed a multiplexed CL detection platform by integrating multiple PCDTBT OPDs with a high-throughput microfluidic chip. The fabricated device is compatible with mass production methods. The analytical performance of the OPD pixel was characterised for the detection of individual waterborne pathogens. *Article IV* performed a series of parallel CL detection experiments to demonstrate the simultaneous detection of multiple waterborne pathogens in one water sample. Rapid multiplexed analysis and extension to complex samples were demonstrated.

Article V investigated the enhancement of CL detection by incorporating standard gold nanoparticles into a simple, inexpensive opto-microfluidic device. The limit of detection for an environmentally relevant protein analyte was ~200 times lower than previously reported CL sensors using other OPD designs. The remarkable stability and specific detectivity of the PCDTBT OPD was also characterised.

Article VI presented a high-efficiency bio-analyte recovery system by incorporating multiple counter-flow filtration units. A high concentrating ratio was obtained with a short processing time. The filtration system showed recovery efficiencies above 80% for waterborne protozoa at environmentally realistic concentrations in real environmental water samples. A compact filter made of multiple counter-flow units arranged into a cascade-like structure is also shown. The separation of water particulates from the target protozoan organisms was addressed to enhance the recovery performance of conventionally used filters.

Preface

This thesis is submitted in candidacy for the degree of Philosophiae Doctor from the Department of Micro- and Nanosystems Technology (IMST) at Buskerud and Vestfold University College (HBV).

The doctoral work has been conducted from August 2011 to March 2014 with Associate Professor Tao Dong, Ph.D. as the primary supervisor.

This work was also supported by co-supervisors Professor Nils Høivik, Ph.D. and Professor Ulrik Hanke, Ph.D.

Financial support was provided by the KD program (proj. no. 08673) at IMST-HBV. Additional support was provided by the Oslofjord Fund (proj. no. 220635 and proj. no. 229857), the Norwegian Micro- and Nanofabrication Facility, Norfab (197411/V30), and the Norwegian PhD Network on Nanotechnology for Microsystems, Nanonetwork (190086, S10).

Acknowledgements

I would like to express my deepest appreciation and my greatest gratitude to my primary supervisor, Associate Professor Tao Dong, Ph.D., for his guidance and valuable advice during my Ph.D. candidature. I am especially grateful for his tireless supervision, motivation and priceless support and suggestions on my scientific work. Furthermore, I thank him for nurturing my ambition and potential as a researcher.

I am very grateful to my co-supervisors, Professor Nils Høivik, Ph.D. and Professor Ulrik Hanke, Ph.D., for their useful discussions on my work. Their clear and precise advice helped me a lot during my Ph.D. candidacy period.

Through the coordinating efforts of my primary supervisor, my Ph.D. research has been supported by several universities/institutions in China: the Henan University of Technology, the School of Mechanical Engineering at Nanjing University of Science and Technology, the Pen-Tung Sah Micro- Nanotechnology Research Center at Xiamen University, the Integrated Detection & Control System Engineering Key Laboratory at Chongqing Technology and Business University, the Suzhou Institute of Nano-Tech and Nano-Bionics and the Institute of Hydrobiology, both at Chinese Academy of Sciences. Here, I would like to thank these institutions for their professional assistance related to device fabrication, device performance characterisation and biological testing.

I would also like to give my sincere thanks to Zekija Ramic and Ragnar D. Johansen of IMST-HBV, and Anand Summanwar and Andreas Vogl of SINTEF MiNaLab for their useful discussions on the challenges of my experimental work.

My appreciations are not forgotten for my friends, Zhaochu Yang, Ph.D., Ph.D. candidate Xinyan Zhao, Ph.D. candidate Haakon Karlsen, master’s student Carlos Honrado and master’s student Cátia Barbosa, for encouraging me during my doctoral work.

Last, but not least, my deepest thanks and sincere gratitude are extended to my family members and close friends in Portugal. I could not have gone this far in my academic journey without their unconditional understanding and support.

List of articles

Papers are not available in this file due to publisher's restrictions

The thesis is based on the following articles:

I. Nuno Miguel Matos Pires, Tao Dong, Ulrik Hanke and Nils Hoivik, Integrated optical microfluidic biosensor using a polycarbazole photodetector for point-of-care detection of hormonal compounds, *Journal of Biomedical Optics*, 18(9)2013, 097001.
My contribution: Design, Part of Experiment, Data analysis, Manuscript preparation

II. Nuno Miguel Matos Pires and Tao Dong, Measurement of salivary cortisol by a chemiluminescent organic-based immunosensor, *Bio-Medical Materials and Engineering*, 24(1)2014, 15-20.
My contribution: Design, Part of Experiment, Data analysis, Manuscript preparation

III. Nuno Miguel Matos Pires and Tao Dong, Multiplexed detection of waterborne pathogens with an array of microfluidic integrated high-sensitivity organic photodiodes, *Proceedings of 2013 IEEE Biomedical Circuits and Systems Conference (BioCAS)*, 2013, 105-108.
My contribution: Conception, Data analysis, Manuscript preparation

IV. Nuno Miguel Matos Pires and Tao Dong, Microfluidic biosensor array with integrated poly(2,7-carbazole)/fullerene-based photodiodes for rapid multiplexed detection of pathogens, *Sensors,* 13(12)2013, 15898-15911.
My contribution: Part of Experiment, Data analysis, Manuscript preparation

V. Nuno Miguel Matos Pires and Tao Dong, Ultrasensitive opto-microfluidic immunosensor integrating gold nanoparticle-enhanced chemiluminescence and highly stable organic photodetector, *Journal of Biomedical Optics*, 19(3)2014, 030504.
My contribution: Design, Part of Experiment, Data analysis, Manuscript preparation

VI. Nuno Miguel Matos Pires and Tao Dong, Recovery of Cryptosporidium and Giardia organisms from surface water by counter-flow refining microfiltration, *Environmental Technology*, 34(17)2013, 2541-2551.
My contribution: Part of Experiment, Data analysis, Manuscript preparation

Additional publications not enclosed in this thesis:

VII. Nuno Miguel Matos Pires and Tao Dong, Detection of stress hormones by a microfluidic-integrated polycarbazole/fullerene photodetector, *Conference*

Proceedings of IEEE Engineering in Medicine and Biology Society, 2013, 4470-4473.

My contribution: Design, Data analysis, Manuscript preparation

VIII. Nuno Miguel Matos Pires and Tao Dong, On-site monitoring of steroid hormones in environmental waters with a low-cost, integrated polymer lab-on-chip device, *Applied Mechanics and Materials*, 448-453 2014, 396-401.

My contribution: Part of Experiment, Data analysis, Manuscript preparation

IX. Nuno Miguel Matos Pires and Tao Dong, An integrated passive-flow microfluidic biosensor with organic photodiodes for ultra-sensitive pathogen detection in water, *Accepted/In press for Conference Proceedings of IEEE Engineering in Medicine and Biology Society*, 2014.

My contribution: Conception, Data analysis, Manuscript preparation

X. Nuno Miguel Matos Pires, Tao Dong, Zhaochu Yang, Nils Hoivik and Xinyan Zhao, A mediator embedded micro-immunosensing unit for electrochemical detection on viruses within physiological saline media, *Journal of Micromechanics and Microengineering*, 21(11)2011, 115031.

My contribution: Design, Part of Experiment, Data analysis, Manuscript preparation

XI. Nuno Miguel Matos Pires and Tao Dong, A cascade-like silicon filter for improved recovery of oocysts from environmental waters, *Environmental Technology*, 35(6)2014, 781-790.

My contribution: Conception, Data analysis, Manuscript preparation

XII. Nuno Miguel Matos Pires and Tao Dong, Biomedical micro-refinery system for the enrichment of Giardia cysts in source water, *Proceedings of 2012 5th International Conference on Biomedical Engineering and Informatics (BMEI)*, 2012, 825-829.

My contribution: Part of Experiment, Data analysis, Manuscript preparation

XIII. Nuno Miguel Matos Pires and Tao Dong, Increasing the protozoan recovery for biomedical membrane filters using multiplexed refining device, *Proceedings of 2012 5th International Conference on Biomedical Engineering and Informatics (BMEI)*, 2012, 830-834.

My contribution: Design, Part of Experiment, Data analysis, Manuscript preparation

Table of contents

Abbreviations

APTES	*(3-aminopropyl)triethoxysilane*
AuNP	*Gold nanoparticle*
CCD	*Charge-coupled devices*
CL	*Chemiluminescence*
CMOS	*Complementary metal-oxide-semiconductor*
*D**	*Specific detectivity*
EDC	*1-ethyl-3-[3-dimethylaminopropyl] carbodiimide hydrochloride*
ELISA	*Enzyme-linked immunosorbent assay*
EQE	*External quantum efficiency*
HRP	*Horseradish peroxidase*
IMS	*Immunomagnetic separation*
IFM	*Immunofluorescence microscopy*
ITO	*Indium tin oxide*
LED	*Light emitting diode*
LOC	*Lab on a Chip*
MEMS	*Micro-electromechanical systems*
NEP	*Noise-equivalent power*
NHS	*N-hydroxysuccinimide*
OPD	*Organic photodiode*
PBS	*Phosphate-buffered saline*
$PC_{60}BM$	*[6,6]-phenyl-C_{61}-butyric-acid methyl-ester*
PCDTBT	*poly[N-9′-heptadecanyl-2,7-carbazole-alt-(4′,7′-di-2-thienyl-2′,1′,3′-benzothiadiazole)]*
PDMS	*Polydimethylsiloxane*
PEDOT:PSS	*Poly(3,4-ethylenedioxythiophene): polystyrene sulfonate*
PMMA	*Poly(methyl methacrylate)*
PMT	*Photomultiplier tube*
POC	*Point-of-care*
P3HT	*Poly(3-hexylthiophene)*
SPR	*Surface plasmon resonance*
μC	*Microconcentrator*

Outline of the thesis

The thesis is organised based on the published articles. The first chapter “Introduction” presents the current status and scope of the research, as well as the motivation for conducting the investigations. In Chapter 2, “Summary of the articles”, six published articles are briefly described and discussed, and each article represents a stage of the work. The presentation of the articles is organised in a systematic way to show the step-by-step progress of the research. The full-length articles are enclosed at the end of thesis. In Chapter 3, “Conclusions”, the scientific contributions of this work are summarised.

1 Introduction

1.1 Background

The detection of pathogens, hormones, or other medically relevant analytes increasingly demands the development of innovative analytical devices with high sensitivity, specificity, precision, speed and usability. Bio-analytes are typically present at very low concentrations in complex/real samples [1], and their detection presents important challenges for current biosensing technologies. These challenges include [2-5]:

- Efficient concentration and recovery of bio-analytes from large-volume samples;
- Highly sensitive and specific detection in samples containing multiple non-targeted particles;
- Multiplexed parallel detection using a simple procedure.

For instance, effective surveillance for waterborne pathogens, such as *Escherichia coli*, rotavirus or *Giardia lamblia*, would require the detection of only 10 to 100 organisms in several litres of sample [6, 7]. Biosensing methods may involve filtration, magnetic separation and optical detection [7-9], all of which are commonly conducted in the laboratory. The laboratory methods, although highly accurate and sensitive, often requires expensive optical instrumentation and labour-intensive sample preparation [10, 11]. Instead, miniaturisation of both filtration and optical detection can be achieved using microfluidics and Lab on a Chip (LOC) technology. Truly miniaturised detection devices are preferred for applications requiring point-of-care (POC) biosensor systems where portability and procedural simplicity are of great relevance [12]. Furthermore, LOCs are widely acknowledged to provide autonomous and rapid analysis [13-15]. In particular, the realisation of low-cost microfluidic methods for both sample filtration and optical detection would have a considerable impact on the fields of clinical diagnostics and environmental monitoring.

1.2 Status of optical detection in lab-on-a-chip devices

Despite recent developments in LOC devices for bio-analyte detection, relatively few successful practical implementations have been demonstrated [16, 17]. Producing cost-effective, portable optical analysis systems for sensitive and specific detection in the micro- or nano-litre sample volumes typically encountered in microfluidic devices remains difficult. Moreover, low power consumption, compactness, automation, and potential for realising multiplex analysis are desirable characteristics for robust POC systems [18, 19]. To demonstrate the practicality of new LOC devices, efforts should be made to incorporate bio-assays amenable for detection in real clinical samples and to compare these new methods´ detection sensitivity to that of conventional methods [20]. Thus, typical methods for optically detecting bio-analytes in LOC devices are discussed in this section. The related techniques and their analytical performance are characterized in Table 1.

Electrochemical assays and micro- and nano-mechanical sensors have been widely employed in microfluidic systems [21-23]. Modern electrochemical biosensors rely on interactions of redox species with the surfaces of particle-modified microelectrodes [24]. These sensors can be easily integrated with microfluidic channels made of polydimethylsiloxane (PDMS) or poly(methyl methacrylate) (PMMA). Moreover, the microelectrodes can be fabricated on simple cellulose-paper substrates using inexpensive screen-printing technology [25, 26]. Electrochemical microfluidic devices are generally considered as cost-effective solutions for rapid analyte detection (~seconds response). Nevertheless, the required labelling of targeted proteins and nucleic acids with electroactive enzymes is a concern. Furthermore, electrochemical methods are commonly affected by temperature variations at the microelectrode, chemical factors (i.e., pH and ionic concentrations), redox by-product accumulation, and electrode surface conditions, which may impose stringent storage conditions for POC devices [27].

In contrast, mechanical cantilever-based biosensors have been successful in the label-free detection of biomarkers and nucleic acids. These sensors generally operate in two different modes: (i) static deflection, where binding on one side of a cantilever causes unbalanced surface stress, resulting in a measurable deflection, and (ii) resonant mode, where binding on a cantilever causes variations in its mass, consequently shifting the

resonant frequency [23]. Cantilever beams are compatible with silicon microfabrication using standard micro-electromechanical systems (MEMS) technology. Further, Au-modified Si cantilevers can be modified with immobilised biomolecules using standard procedures, such as activation by 1-ethyl-3-[3-dimethylaminopropyl] carbodiimide hydrochloride (EDC) and N-hydroxysuccinimide (NHS) [28]. However, the performance of these cantilevers can be affected by temperature fluctuations and other environmental conditions. Although the integration of cantilever technology to LOCs has been successfully demonstrated [29, 30], the detection sensitivity of the resulting devices is limited by losses associated with viscous damping.

Optical method	**Time of analysis**	**Detection limit [ref.]**	**Point of care**	**Comments**
Absorbance	Real time to 12 hours	19.5 ng/mL [38]	High	Reliable method for commercial POC devices
Surface plasmon resonance	Less than 3 hours	5 nM (8 ng/mL) [51]	Low	Robust technique to realise label-free detection
Fluorescence	Real time to 3 hours	2.1 nM (0.6 ng/mL) [41]	Moderate high	Versatile method for molecular sensing due to availability of various dyes
Chemiluminescence	Less than 60 minutes	0.1 ng/mL [56]	Very high	Rapid technique using no complex instrumentation

Table 1: Review of current optical detection methods based on absorbance [17, 36-38], fluorescence [40-43, 45-47], surface plasmon resonance [49-52], and chemiluminescence [53-60] for LOC devices.

The limitations of other techniques have accelerated the development of optical detection for LOC devices. Furthermore, optical instrumentation is ubiquitous in the laboratory, which explains the preference for optical detection in diagnostics [31, 32]. Thus, the realisation of compact, portable detection tools would generate great enthusiasm and acceptance from the clinical personnel. Various optical detection methods, including absorbance, fluorescence, chemiluminescence, and surface plasmon

resonance (SPR), have been exploited in microfluidic biosensors. In general, these methods have been realised in LOCs employing both off- and on-chip photodetectors. In the "off-chip approach" microscopes, spectrophotometers, charge-coupled devices (CCDs) or photomultiplier tubes (PMTs) are coupled [27, 33], while the "on-chip approach" comprises the integration of photodiodes, filters or other micro-optical systems into microfluidic devices [33, 34]. These approaches are summarisd in Table 2. Herein, recent developments in optical microfluidic technologies for bio-analyte detection are discussed.

1.2.1 Absorbance and Fluorescence

Both absorbance and fluorescence are well-established techniques in macroscale analytical chemistry and laboratory diagnostics. Absorbance-based detection measures the attenuation of incident light at a specific wavelength, while fluorescence detects light emission from fluorophores or fluorescent dyes upon excitation by a light source. Light attenuation is conventionally measured by UV absorption spectroscopy, and miniaturisation of this technique is achieved by integrating microfabricated SiO_2 waveguides with microfluidic channels [35]. Other miniaturised absorbance detection systems have been developed by incorporating laser diodes, Si photodiodes or complementary metal–oxide–semiconductor (CMOS) image sensors, and standard PDMS microchannels [36, 37]. In many cases, changes in optical density or colour are sufficient for diagnosis [38]. Opacity changes resulting from the reduction of silver films by gold colloids have been used for biomarker antibody detection [Fig. 1(a)], and these simple inexpensive immunoassays have been exploited in commercial POC devices [17].

Fluorescence detection often requires an excitation light source, a fluorophore to label proteins or nucleic acids, wavelength filters to isolate emission photons from excitation photons, and a detector that registers emission photons and produces a recordable output, generally an electrical signal. This configuration is commonly encountered in integrated microfluidic devices [39, 40], where light-emitting diodes (LEDs) can be used as excitation light sources, and CMOS image sensors can be used as photodetectors [Fig. 1(b)]. While externally mounted microscopes, microplate readers and CCD cameras are still used to interrogate the microfluidic chip [41-43], organic photodiodes (OPDs) are emerging photodetectors for integration with LOCs. The benefits of OPDs include, an uncomplicated optical alignment, thin device architecture

(< 1 μm), variable size of the active area (ranging from cm^2 to mm^2) and substrate independence [44].

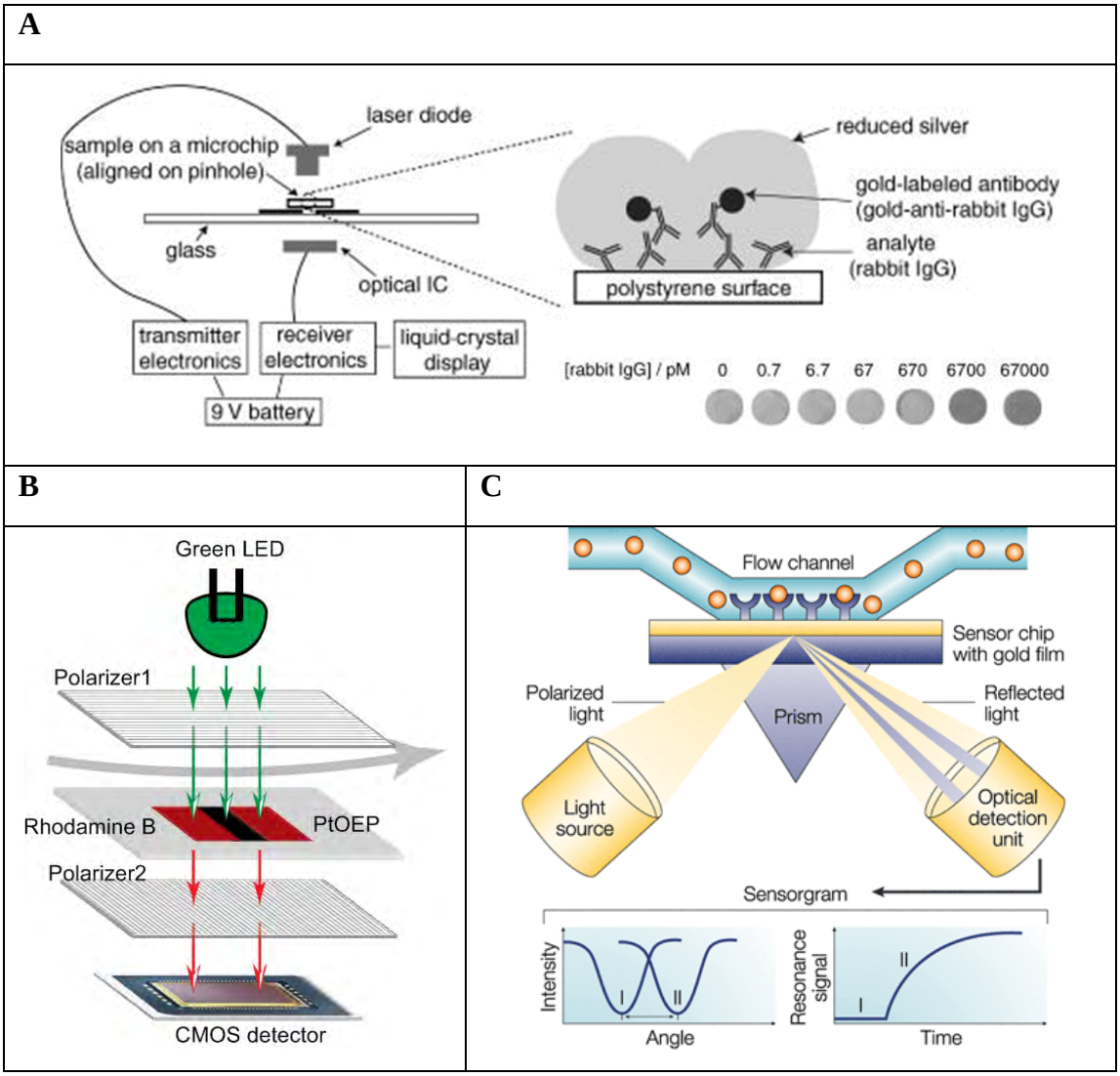

Fig. 1. Methods of absorbance, fluorescence and SPR based detection. (A) Schematic of a compact absorbance-based biosensor [36]. An incorporated laser diode illuminates a silver film whose reduction by gold colloids changes the film opacity. The apparent absorbance is measured by an optical IC incorporating a Si photodiode. (B) Arrangement of a fluorescence-based oxygen detection system containing an oxygen sensitive PtOEP film, oxygen insensitive Rhodamine B film, CMOS detector, LED and polarizer filters [40]. (C) Setup of a SPR system for microfluidic detection [48]. Refractive index changes due to binding of bio-analytes to an antibody-modified Au film are detected by a coupling system of a light source, prism and optical detector.

OPDs made of CuPC and C_{60} have been used as photodetectors for the fluorescence detection of Rhodamine 6G, resorufin and fluorescein dye in compact LOCs [45, 46]. These OPDs are fabricated via the thermal evaporation of CuPC/C_{60} onto 100-nm-thick indium tin oxide (ITO) coatings on glass slides previously patterned by a wet etching process. Further, 100-nm-thick Al or 50-nm-thick Ag strips are deposited on top of the

polymer film, followed by encapsulation of the fabricated OPD substrate with a glass substrate using a UV-cured adhesive. The thicknesses of CuPC and C_{60} are typically 20-57 nm and 35-60 nm, respectively, and they can be controlled by adjusting the time and deposition rate for the evaporation process.

Although fluorescence detection may be compatible with capillary flow based microfluidic schemes that preclude the use of external pumps and valves [42], its performance can be affected by autofluorescence of non-specific biomolecules in the sample. Furthermore, both fluorescence and absorbance suffer at smaller geometries because the optical path length through the sample is shortened, as described by the Beer-Lambert law [27, 47].

1.2.2 Surface plasmon resonance

SPR is based on the detection of a refractive index change at a thin metal film (typically Au). The binding of bio-analytes to biomolecule-functionalised Au thin film causes a shift in the resonant angle when a propagating surface plasmon at the Au film is excited by an incident light source [48]. This mechanism is summarized in Fig. 1(c). Although SPR is most likely to be conducted in the laboratory, efforts have recently focused on the miniaturisation of SPR sensors by incorporating microfluidics. While microfluidic cells have been incorporated in commercial SPR instruments (equipped with LEDs, prisms and CCD sensors) [49], miniaturised SPR biosensors have been developed by integrating Au waveguides with standard microfluidic channels [50].

The SPR setup is compatible with “sandwich” immunoassays [51] using nanoparticle-based amplification [49]. Moreover, metal nanoparticles can be exploited for localised SPR, where the resonant oscillation of conducting electrons at the nanoparticle surface occurs under the perturbation of incident light. This concept of SPR prevents the use of prisms or grating couplers [52]. However, externally mounted CCDs are still employed in recently reported SPR sensors, which limits the implementation of these sensors in POC systems. Furthermore, SPR performance can be hindered by temperature variations.

1.2.3 Chemiluminescence

In chemiluminescence (CL), analyte binding causes photochemical emission, either directly or through the use of an enzyme label. CL detection does not require an

excitation light source or emission filters, which greatly decreases the cost and complexity of the necessary instrumentation. A number of CL reaction types have been exploited in LOC devices, including CL of horseradish peroxidase (HRP) and 3,3`,5,5`-tetramethylbenzidine substrate [53], and CL of HRP and luminol/H_2O_2/enhancer cocktail [54]. Moreover, these CL methods are often combined with classical enzyme-linked immunosorbent assays (ELISAs). In microfluidic CL assays, emitted light is conventionally transduced into an electrical signal with either a PMT [Fig. 2(a)] [55] or a CCD [56, 57]. The use of CCD technology may ensure the realisation of versatile analytical devices for a wide range of protein and nucleic acid analytes [Fig. 2(b)], despite the high costs of its miniaturisation.

The low-cost miniaturisation of microfluidic CL detection systems would be of great value for the development of disposable LOCs for POC settings. Arrays of hydrogenated amorphous silicon (a-Si:H) photodiodes have been popularised as integrated photodetectors for microfluidic CL detection [58, 59]. A schematic of a-Si:H sensor integration to a PDMS microfluidic channel is depicted in Fig. 2(c). The fabrication of a-Si:H photodiodes involves plasma enhanced chemical vapour deposition of multiple a-Si:H layers onto patterned transparent oxide films. This process is followed by sputter coating with three metal layers (Cr/Al/Cr) and then patterning the device structure using a number of wet and reactive ion etching processes. In addition, a-Si:H devices are commonly insulated with thick SU8 layers. This process flow is in contrast to the inexpensive preparation of OPDs on glass or polymer substrates using simple spin-coating, inkjet printing or spray-coating techniques [44].

Blend heterojunction OPDs of poly(3-hexylthiophene) (P3HT) and (6,6)-phenyl C_{61} butyric-acid methyl-ester ($PC_{60}BM$) have been developed for microfluidic CL sensors with PDMS microchannel integration [60-63]. Fig. 2(d) depicts the structure of the integrated P3HT:$PC_{60}BM$ OPD that was used to monitor CL reactions of peroxyoxalate with H_2O_2 in the presence of 9,10-diphenylanthracene. The fabrication of this OPD was conducted as follows [63]: (1) spin coating of a 60- to 100-nm-thick layer of poly(3,4-ethylenedioxythiophene):polystyrene sulfonate (PEDOT:PSS) onto a 0.7- to 1-mm-thick glass substrate coated with ~100 nm ITO; (2) deposition of a 150-nm-thick active layer of P3HT and $PC_{60}BM$ by spin-coating a 1:1 blend of the two components in dichlorobenzene; and (3) deposition of a thermally evaporated 100- to 200-nm-thick layer of Al onto the polymer film under vacuum conditions. Additional fabrication steps

include photodiode annealing in a dry N_2 atmosphere and device encapsulation using a UV-cured adhesive. The integrated microfluidic device is assembled by attaching the uncoated side of the OPD substrate to the surface of a PDMS microfluidic layer previously fabricated by standard soft lithography [10].

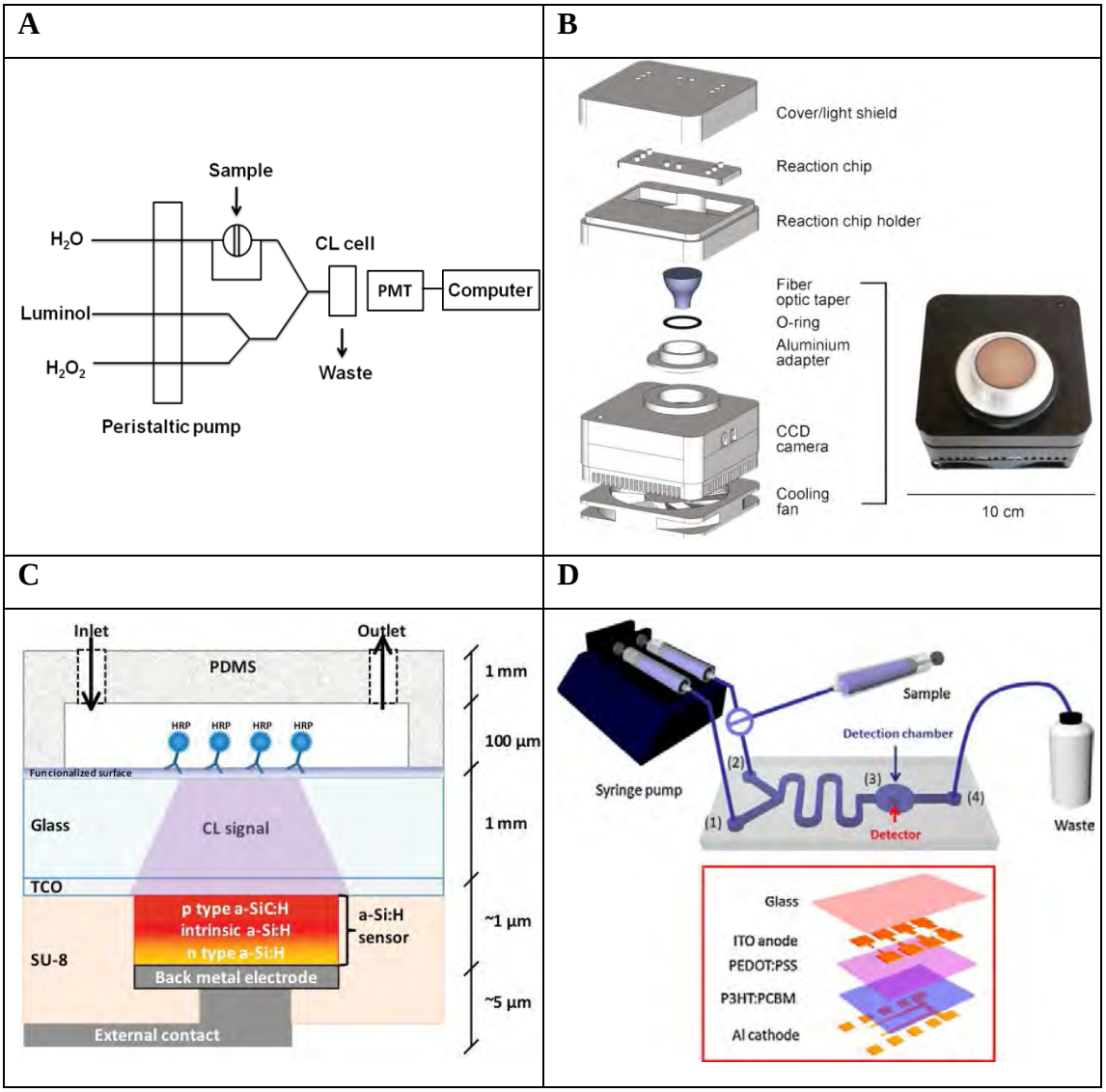

Fig. 2. Methods of CL detection in microfluidic systems. (A) Schematic of a flow injection system for CL analysis using PMT technology [55]. (B) Microfluidic device incorporating a thermoelectrically cooled CCD camera for monitoring CL reactions of various types [57]. (C) Integrated opto-microfluidic sensor with a hydrogenated amorphous silicon (a-Si:H) photodetector prepared onto a glass substrate covered by a transparent conductive oxide (TCO) film [59]. (D) Integration of an organic P3HT:PCBM photodetector to a CL reaction chamber [62]. Two inlets (1 and 2) and one outlet (4) were arranged in a microfluidic channel containing the detection zone (3).

Using the CL system of HRP/luminol/H_2O_2, which is used in immunoassays, the integrated P3HT:PC_{60}BM OPD detected a pathogen toxin with a resolution of 500 pg/mL [60]. This value is in contrast to the 100 pg/ml detection limit achieved with a

CCD camera [56]. In addition, the CuPC/C_{60} OPD was employed in microfluidic CL immunoassays and demonstrated a detection limit of 16 ng/mL [46].

Integration	Photodetector	Merits	Drawbacks
Off-chip	PMTs	Generally show superior detection sensitivity, and precision; Variety of commercially available instruments.	High complexity, high cost and high power consumption; Limited use in compact portable sensors for POC aplications.
	CCDs		
	Microplate readers and microscopes		
On-chip	Si photodiodes	High detection sensitivity in integrated microfluidic devices.	The complexity of their fabrication makes them too expensive for disposable sensors.
	CMOS image sensors		
	OPDs	Simple, low-cost fabrication on glass or polymer substrates.	Performance still inferior to Si photodetectors.

Table 2: Summary of photodetectors currently employed in microfluidic detection of proteins and pathogens. Merits and drawbacks of the detector technologies are described for both off-chip [60, 62] and on-chip [60, 61] integration to microfluidics.

1.3 Mechanisms of bio-analyte recovery

The detection of bio-analytes commonly involves the analysis of low target concentrations in the initial sample. Therefore, initial sample preparation is of high importance for achieving high sensitivity and specificity in any optical detection system. The enrichment/recovery of the target analyte and/or the removal of inhibitors are common strategies in this regard. This preparation is especially important in systems dealing with complex matrices, such as blood, saliva, urine, and environmental water samples composed of many different entities. Furthermore, optical detection can demand the recovery of organisms from large volumes of sample. For instance, the recovery of waterborne bacteria, protozoa and viruses requires that 10 to 100 L of a water sample be concentrated to hundreds or tens of mL for further optical analysis [64, 65]. Table 3 summarises the typical techniques used to separate and concentrate bio-analytes in liquid samples.

The application of dielectrophoresis (DEP) has been demonstrated for the separation and concentration of multiple bio-analytes, including protozoa, bacteria, viruses, human cells, and large strands of nucleic acids [66, 67]. DEP is an electrokinetic phenomenon involving the interaction of an inhomogeneous electric field with polarisable particles. The polarisability of the target particles in their surrounding medium induces dielectrophoretic motion towards or away from the electrode surface. The strength of the DEP force depends on the electrical properties, the shape and size of the target particles, and the frequency of the electric field. With DEP, liquid samples can be continuously processed in microfluidic chips [66, 68]. Furthermore, single organisms can be manipulated in a non-invasive manner, and the method provides selectivity between viable and non-viable biological cells [69]. However, the varying conductivity of samples poses a challenge to the use of DEP systems in real-world applications. Standardisation of medium conductivity by sample pre-treatment may be necessary when DEP performance based on the differences in polarisability between the target particles and the medium has been established. Moreover, clogging is likely to occur in DEP separators, and the method is only capable of processing up to mL volumes of biological and water samples [68]. Samples comprising tens or even hundreds of litres can be processed by sedimentation [70] and centrifugation [70, 71] based separation methods. With sedimentation, the target organisms are separated from the medium as an insoluble precipitate. With centrifugation, the organisms are collected in circular channels by applying centrifugal forces. The precipitation of non-targeted particulates is a major concern for sedimentation, while the centrifugal separation is often costly and can damage cells. Both separation methods are also limited by lengthy process times [70, 71].

Filters are a cost-effective and straightforward alternative for the rapid recovery of bio-analytes from liquid samples. Dead-end membrane filters have been made from polycarbonate, cellulose acetate and silicon [32, 72-74]. In these filters, particles larger than the pore size are retained in the membrane, while smaller particles pass through the membrane. Using this size-exclusion principle, silicon-micromachined filters have been shown to recover protozoan organisms, but only in 10 mL of pure water [74]. The filtration of tens or even hundreds litres of complex water samples hinders the recovery performance of membrane filters. Solid particulates in turbid waters adhere to the filter surface, potentially leading to clogging and failure of the filters.

Technique	Principle	Recovery rate [ref.]	Characteristics
DEP	Phenomenon acting on polarisable particles in a non-uniform electric field, used to collect or trap these particles.	~100% [67]	Selective separation of a wide range of bio-analytes and continuous target enrichment at low flow rates.
Sedimentation	It involves transformation of dissolved or suspended matter into an insoluble solid (containing the target analyte).	Up to 77% [70]	Precipitation of non-targeted particles impact the process efficiency.
Centrifugal separation	Targeted particles are retained in fluidic channels due to centrifugal force.	49 to 71% [71]	Continuous-flow separation of targeted organisms despite its lengthy process times.
Filtration	Relies upon the size of the targeted organism to separate it from other particules existing in the sample.	Above 80% [76]	Superior recovery performance is achieved by processing small sample volumes.
Magnetic bead separation	Analyte capturing by probe-functionalized beads that are further isolated by a magnet.	~95% [78]	Method for high selectivity separation of bio-analytes in milliliter volumes of sample.

Table 3: Summary of techniques widely used for bio-analyte recovery, including DEP [66-69], sedimentation [70], centrifugation [70, 71], filtration [72-77] and magnetic bead separation [78-80]. These separation methods are compatible with conventional optical detection.

Cross-flow filtration has also been exploited in bio-analyte recovery. Using this method, sample flows tangentially across the filter surface rather than into the filter, which is the case for dead-end filtration. Microbial cell recovery was demonstrated by employing silicon cross-flow filters [75], and water enrichment has been shown using hollow fibre cross-flow separators [64, 65]. Recoveries exceeding 80% may be achieved by cross-flow devices when filtering 2 L samples of environmental water [76]. However, the filtration of 10 L of environmental water could result in a 30% reduction in the recovery performance [64]. In most cases, laborious elution steps are involved in the collection of

the target organisms from the filter surface. Moreover, cross-flow filtration is typically performed with reusable devices which have limited application for cases where cross-contamination is of particular concern. The enrichment of human cells was demonstrated using counter-flow microfiltration, which is a derivation of the cross-flow principle. Counter-flow filtration has recently been achieved in a silicon-micromachined concentrator device [77], and its merits of non-clogging and high processing efficiency may encourage its use in water particle recovery.

Magnetic bead separation is widely used in bio-analyte recovery and isolation, exploiting the unique advantages of paramagnetic beads, which include high surface-to-volume ratio, facile functionalisation with biochemical probes, and easy handling through the use of magnets. Magnetic beads functionalised with antibodies have been successfully applied in protein and pathogen detection [78, 79]. In this approach, the target organisms are captured by immunomagnetic beads within a solution in the presence of magnetic field. Although immunomagnetic separation (IMS) is often performed with samples in the μL to mL volume range, its high selectivity and high recovery efficiency encourage the combination of IMS with filtration methods for large volume sample processing [78]. For instance, the detection of protozoan organisms in environmental water commonly involves the use of IMS after filtration of 10 L or 100 L water samples, where IMS is combined with immunofluorescence, a standard optical detection method [80].

1.4 Aims and Tasks

From the literature survey, it was concluded that opto-microfluidic systems demonstrate remarkable bio-analyte detection performance, which warrants further investigation, and provides strong motivation for the large number of researchers currently working in this field. The detection sensitivity and device cost-effectiveness are two key factors restricting the application of opto-microfluidic systems in POC settings. To enhance POC application, employing CL assays that do not require complex instrumentation and developing optical detectors using low-cost micro/nanofabrication are straightforward strategies. Furthermore, the sensitivity of optical detection can be improved by applying methods of assay enhancement and sample preparation. In this thesis, the research has focused on two fields: optical microfluidic biosensor development and bio-analyte recovery.

The first aim of this thesis is to realise cost-effective and high performance opto-microfluidic devices by developing high detectivity, high stability photodetectors based on semiconducting polymers and then integrating these photodetectors with microfluidic structures. The main tasks involved in this aim include the following:

T1. Review of the application of OPDs to optical biosensors, including study of detector configuration and fabrication.
T2. Develop an OPD based biosensor for protein and pathogen detection in microfluidic environments.
T3. Perform CL detection tests and analyse device performance in terms of its detection limit, sensitivity, specificity and reproducibility.
T4. Realise parallel bio-analyte detection in a microfluidic system by employing multiple OPD pixels.
T5. Explore mechanisms for enhancing the detection sensitivity of OPD-based CL biosensors.

The second aim is to develop particle recovery systems by exploiting the counter-flow microfiltration method. The tasks for this aim include the following:

T6. Review and analyse the theory of the passive filtration systems applied to waterborne pathogen recovery, including the study of filtration principles, device configuration and device cost-effectiveness.
T7. Develop continuous-flow water particle separation devices for processing large volumes of complex samples.
T8. Characterise the recovery performance of the developed particle separation systems using standard optical detection.

1.5 Contributions of the thesis

The aforementioned research tasks were all performed together with the primary supervisor, who has been the intermediary for support provided by the Henan University of Technology (HUT), the School of Mechanical Engineering at Nanjing University of Science and Technology (NUST), the Pen-Tung Sah Micro- Nanotechnology Research Center at Xiamen University (XMU), the Integrated Detection & Control System Engineering Key Laboratory at Chongqing Technology and Business University (CTBU), the Suzhou Institute of Nano-Tech and Nano-Bionics (SINANO) and the

Institute of Hydrobiology (IHB), both at Chinese Academy of Sciences. The device design and characterisation were performed in cooperation with the primary supervisor. Device fabrication and packaging were partly performed by the candidate and partly conducted at SINANO, XMU and CTBU. The experimental testing was performed with assistance from HUT, NUST, CTBU, and IHB, and all data analyse and interpretations were conducted by the candidate.

The main scientific contributions of this work are as follows:

C1. An integrated opto-microfluidic biosensor concept for CL detection using an OPD with enhanced characteristics of quantum efficiency and dark current while retaining simple, inexpensive fabrication.

C2. A discovery of the effect of photoactive layer thickness and hole transport layer thickness of the OPD on CL detection sensitivity.

C3. A demonstration of the opto-microfludic biosensor mentioned above for quantitative CL immunoassay detection.

C4. Characterisation of the analytical performance (i.e., linearity, sensitivity, resolution specificity, reproducibility) of the integrated OPD for the detection of a clinically relevant protein analyte.

C5. A low-cost biosensor array integrating a hybrid microfluidic chip and a substrate with multiple OPD pixels.

C6. Simple method of permanent assembly for the hybrid microfluidic chip that enables the covalent binding of antibodies.

C7. A demonstration of the low-cost biosensor array mentioned above for parallel monitoring of CL immunoassays to simultaneously detect multiple pathogens.

C8. A simple ultrasensitive CL immunosensor exploiting the CL enhancing effect of nanoparticles and the high detection sensitivity of the above OPD.

C9. A discovery of the stability of CL detection response under ambient conditions without applying encapsulation to the above OPD.

C10. An enhanced pathogen recovery system employing multiple counter-flow filtration units to process large-volume complex water samples.

C11. Compact particle refining system with outstanding ability for water particulate pre-separation. Demonstration of recovery performance enhancement for standard filters using the refining system as a pre-filter.

These achievements have been reported in internationally published conference and journal papers. A detailed summary of the papers that form the basis of this thesis is presented in Chapter 2. All manuscripts were diligently prepared by the candidate with revisions provided by the co-authors.

2 Summary of the articles

In this section, six articles are selected to highlight the research contributions of the doctoral work. The research consists of three distinct directions: (1) investigation of CL detection performed by an integrated OPD pixel in Article I and Article II; (2) realization of parallel CL detection employing a multiplexed OPD sensor in Article III and Article IV; and (3) investigation of strategies to enhance opto-microfluidic detection sensitivity in Article V and Article VI. The collected articles are organised according to the research stage, rather than the publication date. The full-length articles are enclosed at the end of this thesis.

2.1 Chemiluminescent detection by PCDTBT:$PC_{70}BM$ pixel

2.1.1 Design and fabrication of an integrated OPD pixel (Article I)

The development of OPD-integrated microfluidic systems is still in an early stage. Further investigation may focus on developing OPDs with improved sensitivity. Recent advances on semiconducting polymers have produced novel photoactive materials with enhanced optoelectronic characteristics [81]. Among them, poly[N-9′-heptadecanyl-2,7-carbazole-alt-5,5-(4′,7′-di-2-thienyl-2′,1′,3′-benzothiadiazole)] (PCDTBT) have been combined with $PC_{70}BM$ to form heterojunction devices exhibiting higher photon collection efficiencies and lower dark currents compared with P3HT:$PC_{60}BM$ based OPDs [82]. These unique characteristics may enhance the detection sensitivity of OPD microfluidic biosensors. Blend heterojunction devices of PCDTBT:$PC_{70}BM$ have been reported to be promising organic solar cells with superior power conversion efficiencies [83]. However, their higher sensitivity to light has not yet been exploited for microfluidic assays. In this work, a PCDTBT:$PC_{70}BM$ OPD was developed and integrated to a PDMS-Au-glass hybrid chip for microfluidic CL detection. The motivation was to develop a miniaturised, low-cost but highly sensitive opto-microfluidic biosensor for POC application.

Principle

A scheme of the opto-microfluidic biosensor is shown in Fig. 3. The integrated OPD comprises the ITO/PEDOT:PSS/PCDTBT:$PC_{70}BM$/LiF/Al diode architecture. The active area of the photodetector is aligned with a 30 μL volume reaction chamber on an Au-coated glass microchip. CL sandwich immunoassays are developed on the Au surface. The CL oxidation of luminol by HRP conjugates in the presence of H_2O_2 is used to generate ~425 nm light at an intensity proportional to the amount of analyte targeted by the immunoassay. Light photons are absorbed by the PCDTBT: $PC_{70}BM$ blend heterojunction, resulting in photogenerated electrons and holes collected at the corresponding opaque LiF/Al cathode and transparent ITO anode.

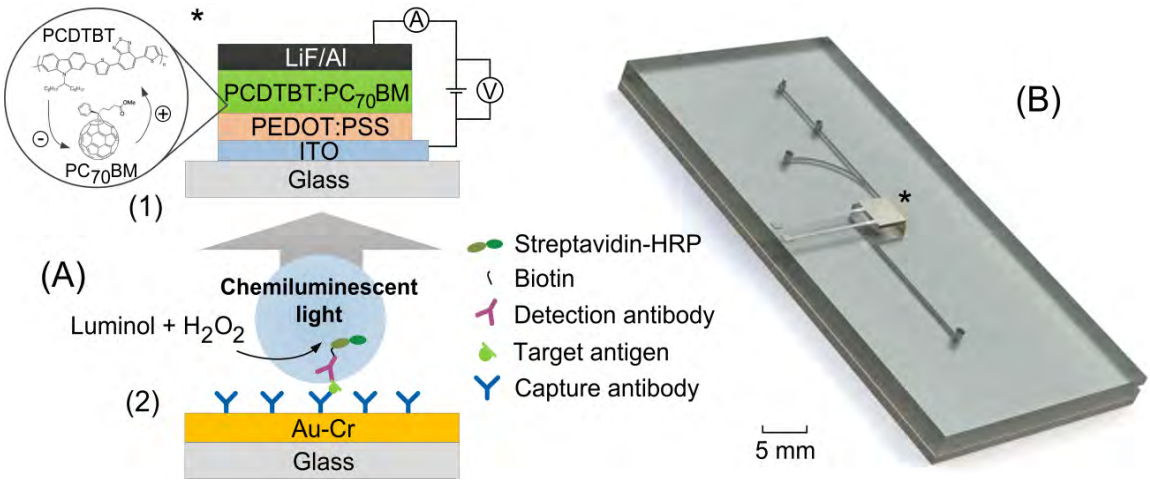

Fig. 3. (a) CL detection scheme showing (1) the design of the PCDTBT:$PC_{70}BM$ OPD and (2) Au-glass chip where CL immunoassays are conducted to detect the target bio-analyte. The generated light is detected as photocurrent by the OPD. (b) Layout of the OPD integrated opto-microfluidic device. The sensing area (4 × 4 mm^2) of the OPD matches to the dimensions of the CL reaction chamber.

Experiments

1. *OPD preparation*

The OPD was prepared on 100-nm-thick ITO coating on glass substrates. After the substrates were pre-treated by UV/ozone, PEDOT:PSS (used as received) was deposited on top of the substrates via spin coating. The thickness of PEDOT:PSS films ranged from 80 nm to 25 nm. PCDTBT (used as received) was dissolved in chloroform to prepare a 4 mg/mL solution, following by blending with $PC_{70}BM$ (used as received). The resultant blends with a mass ratio of 1:4 in chloroform were spin coated onto the

PEDOT:PSS layer, resulting in PCDTBT:$PC_{70}BM$ thicknesses ranging from 70 to 180 nm. The substrates were then transferred to a glove box filled with high purity N_2 and dried at 60°C for 1 h. Furthermore, a LiF/Al electrode (~100 nm) was deposited onto the polymer film by thermal evaporation under a pressure of 3×10^{-4} Pa using a shadow mask. The active area of the OPD, defined by the spatial overlap of the ITO anode and LiF/Al cathode, was 0.16 cm^2. Following fabrication, the OPDs were encapsulated with a customised single-sided pressure-sensitive barrier foil.

2. Microfluidic integration

The microfluidic chip was fabricated by standard PDMS casting. A mixture of Sylgard 184 precursor and a curing agent was degassed in a vacuum and poured onto a SU-8 master template. After curing, the 800-μm-thick PDMS cast was peeled off from the master and the structure of 800-μm-deep chamber was obtained using a scalpel blade. The microchannels connecting the inlets and the chamber were 250 μm wide and 300 μm deep, while the channel connecting the outlet and the chamber was 250 μm wide and 650 μm deep (Fig. 4). This microchannel layer was permanently attached to a 1-mm-thick PDMS slab after exposing the contacting surfaces to oxygen plasma.

The PDMS set was further attached to a Au-coated glass slide by means of carboxylamine coupling chemistry. Prior to attachment, a Pyrex 7740 glass wafer was sputter coated with a 200-nm Au layer using a 20-nm Cr film as an adhesion layer. The Au substrate was cleaned in 5:1 H_2SO_4/H_2O_2 solution, dried in a N_2 atmosphere, and exposed to UV/ozone for 5 min. The clean substrate was immersed in a 10% (v/v) solution of *N*-[(3-trimethoxysilyl)propyl] ethylenediaminetriacetic acid in water for 2 h to develop carboxyl-terminated functional groups on the surface. After three washes with ultrapure water, the substrate was treated with 50 nM NHS and 200 mM EDC for 30 min at room temperature. The bonding surface of the PDMS chip was modified with amine-terminated groups after immersion in a 10% (v/v) solution of (3-aminopropyl)-trimethoxysilane in ethanol for 1 h. The substrate was then washed three times in ethanol. Both the modified PDMS and gold substrates were dried under N_2 for immediate bonding. The PDMS and Au surfaces were finally sealed at room temperature for 1 h. Irreversible attachment was achieved via NHS-EDC coupling chemistry. Additionally, NHS-EDC functionalisation of the Au surface within the reaction chamber allows for the covalent binding of antibodies [84]. To assemble the

integrated opto-microfluidic device, the glass side of the OPD was permanently attached to the lid of the PDMS chip (Fig. 4).

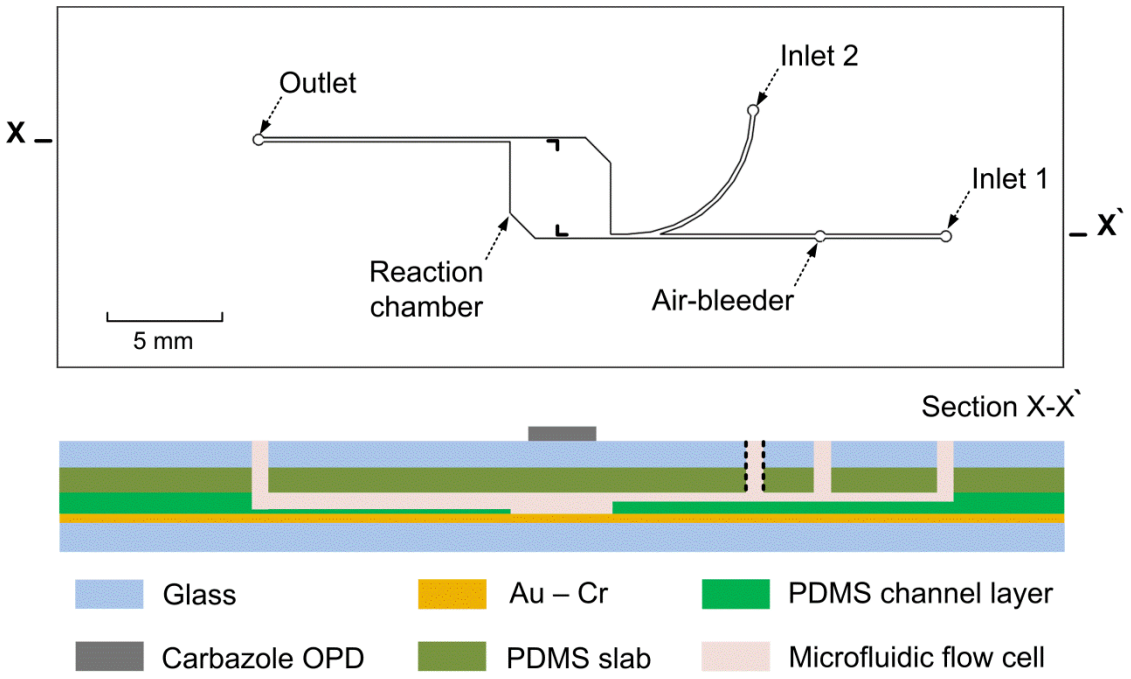

Fig. 4. Top view of the PDMS microchannel layer and side view of the OPD integrated opto-microfluidic device shown in Fig. 3 (layers are not to scale). The device is assembled by attaching the glass side of the OPD to the PDMS slab which is bonded to the PDMS-Au-glass hybrid microchip.

3. Measurement procedure

Fluidic access holes were added to the glass substrate of the OPD, coinciding with the channel inlets (750 µm wide), air-bleeder (750 µm wide) and channel outlet (720 µm wide) in the PDMS layer. Capillary reservoirs were then connected to the entrance of the microchannels. Three OMNIFIT© eight-way valves were used to control the delivery of reagents into the integrated opto-microfluidic device (Fig. 5). Waste was collected by a vacuum flask connected to a micro gear pump. The pressure inside the flask did not exceed 50 kPa during fluid flow operation. Furthermore, small gas bubbles, likely generated at the beginning stage of reagent loading, were removed via the air-bleeder. The OPD photocurrent was measured using a Keithley 236 source measure unit (SMU), and the recorded data were transferred to a PC via a USB-GPIB interface adapter.

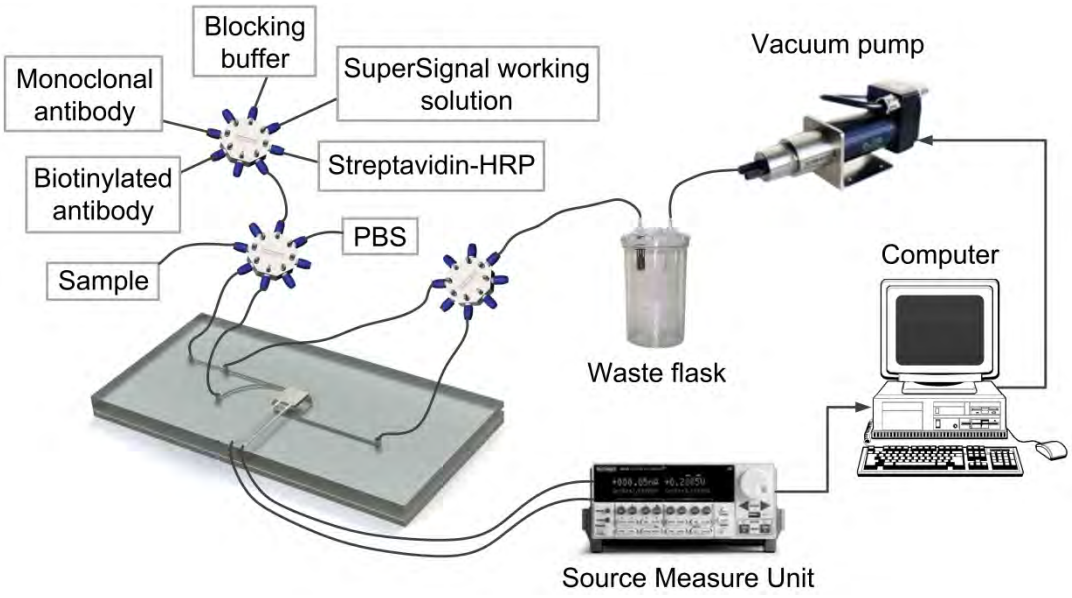

Fig. 5. Schematic of the apparatus for the CL immunoassay experiments.

This setup was used for the CL immunoassay as depicted in Fig. 3(a). The assay was developed after the microchannels and reaction chamber were flushed with phosphate-buffered saline (PBS, pH 7.2), as follows:

(1) Loading a 50 μL aliquot of 0.1 μg/mL capture antibody into the chamber through inlet 1 of the integrated device (Fig. 4), and incubating the antibody solution within the chamber for 2 h.
(2) Washing unbound antibody from the microchip.
(3) Blocking the Au surface with StartingBlock™ blocking buffer, followed by rinsing with PBS for 5 min.
(4) Adding 100 μL of sample to the microchip via inlet 1 and incubating at room temperature for 15 min.
(5) Rinsing the microchip with PBS.
(6) Flushing of 100 μL biotinylated detection antibody into the integrated device for 2 min through inlet 2 (to avoid contamination).
(7) Interaction of the immune complex with streptavidin-HRP conjugate, followed by the addition of luminol/enhancer and stable H_2O_2 solution via inlet 1.

Detection of CL light was conducted in the dark, and all assay components were prepared from 0.01 M PBS before assay development.

Results and discussion

1. *Optimisation of OPD design*

The first CL measurements were conducted to optimise the CL detection sensitivity of the OPD pixel. The transient CL signal measured under short-circuit conditions is shown in Fig. 6(a). This response was obtained by targeting human thyroid-stimulating hormone (TSH), which was used as a model bio-analyte for the CL immunoassay. The sensitivity of OPD-based detection can be enhanced by lowering the dark current and increasing the external quantum efficiency (EQE) for the desired wavelength range [61]. Optimising the thickness of the active layer and hole transport layer represents a promising approach for improving the dark current and EQE characteristics of an OPD [85, 86]. Thus, devices with varied PCDTBT:$PC_{70}BM$ and PEDOT:PSS thicknesses were studied in this work.

Photodetectors with PCDTBT:$PC_{70}BM$ ranging from 70 to 180 nm were first compared. The PEDOT:PSS layer was fixed at 50 nm. Figure 6(a) plots the CL signals measured at varied active layer thicknesses. The average photocurrent at the plateau of the signal (time period between 3 and 7 min) was determined for comparison. A significant increase in the plateau current (I_p) was obtained for PCDTBT:$PC_{70}BM$ with a thickness of 120 nm, which was approximately two-fold higher than that of the 70-nm-thick layer. The changes in I_p were in agreement with the results for EQE [Fig. 6(b)]. Here, EQE was determined from the ratio of the current density collected at the device electrodes to the flux density of incident photons [87]:

$$\mathrm{EQE} = \frac{hcJ_{sc}}{P_0 \lambda q} 100 \qquad (1)$$

where J_{sc} represents the short-circuit current density, P_0 is the incident illumination in W/m^2, λ denotes the incident wavelength, and q is the elementary charge constant. The photocurrent was measured using the Keithley 236 SMU under monochromatic light irradiation. The incident light power was calibrated using a Si photodiode. The EQE values were calculated for incident wavelengths between 400 and 500 nm. An EQE of 62% was obtained for the 120-nm-thick PCDTBT:$PC_{70}BM$ device under monochromatic irradiation at 425 nm. The decreased responses observed in Fig. 6(b) for

the PCDTBT:$PC_{70}BM$ thicknesses between 120 and 180 nm were mainly attributed to the reduced efficiency of charge transport in these thicker layers [88].

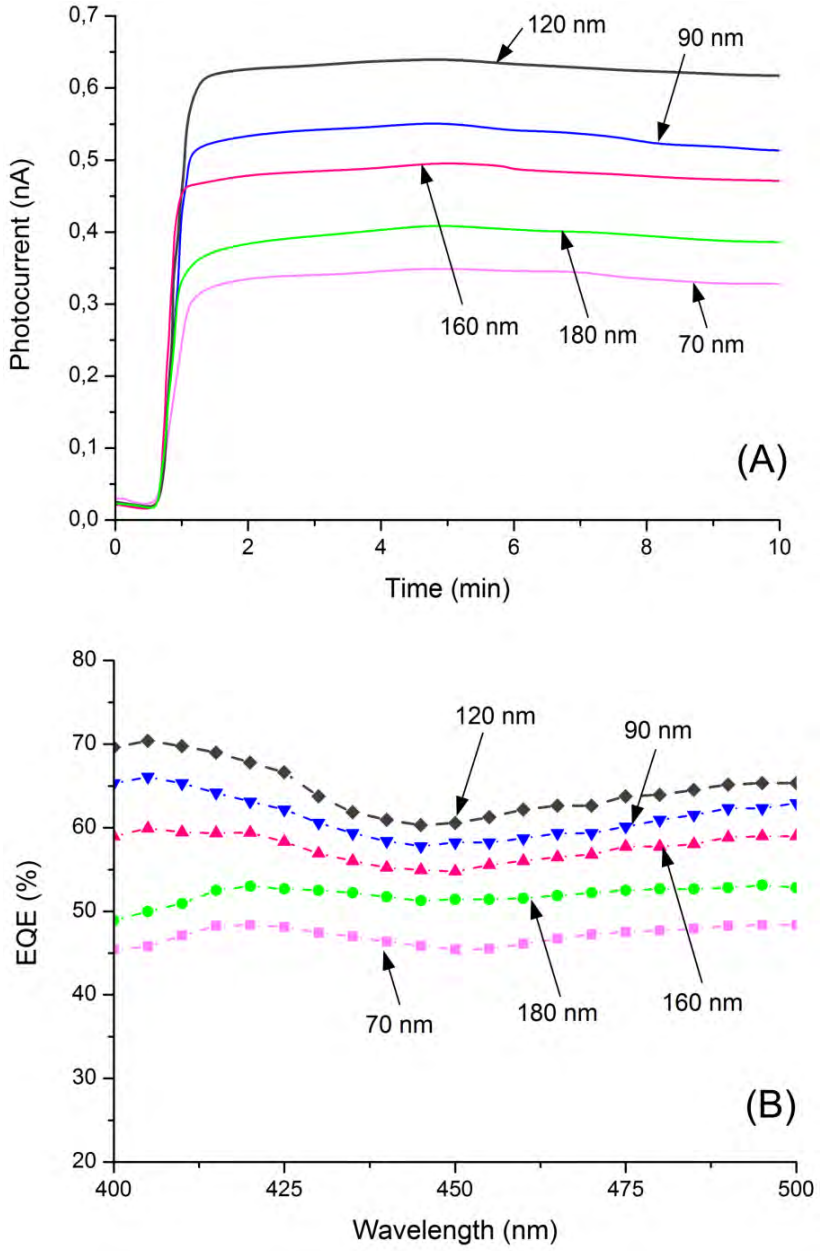

Fig. 6. Experimental optimisation of photoactive layer design. (a) Transient response due to CL detection of 10 ng/mL TSH measured as a function of PCDTBT:$PC_{70}BM$ thickness. (b) EQE spectra for different PCDTBT:$PC_{70}BM$ thicknesses.

Fig. 7(a) shows the background level (I_0) of the OPD as a function of the PEDOT:PSS thickness from 25 to 80 nm, where the PCDTBT:$PC_{70}BM$ layer was maintained at 120 nm. I_0 was measured before performing the assay such that only the effect from the dark current was considered. A minimum background current was observed for the 40-nm-thick PEDOT:PSS when no bias voltage was applied, and the measured value corresponded to an approximately six-fold improvement over the layer thickness of 50

nm. I_p was also enhanced by the 40-nm-thick PEDOT:PSS [Fig. 7(b)]. The decreased thickness of PEDOT:PSS from 80 to 40 nm improved the detector response, which may have resulted from an increased EQE [Ref. 85] and/or enhanced CL light absorption by the OPD.

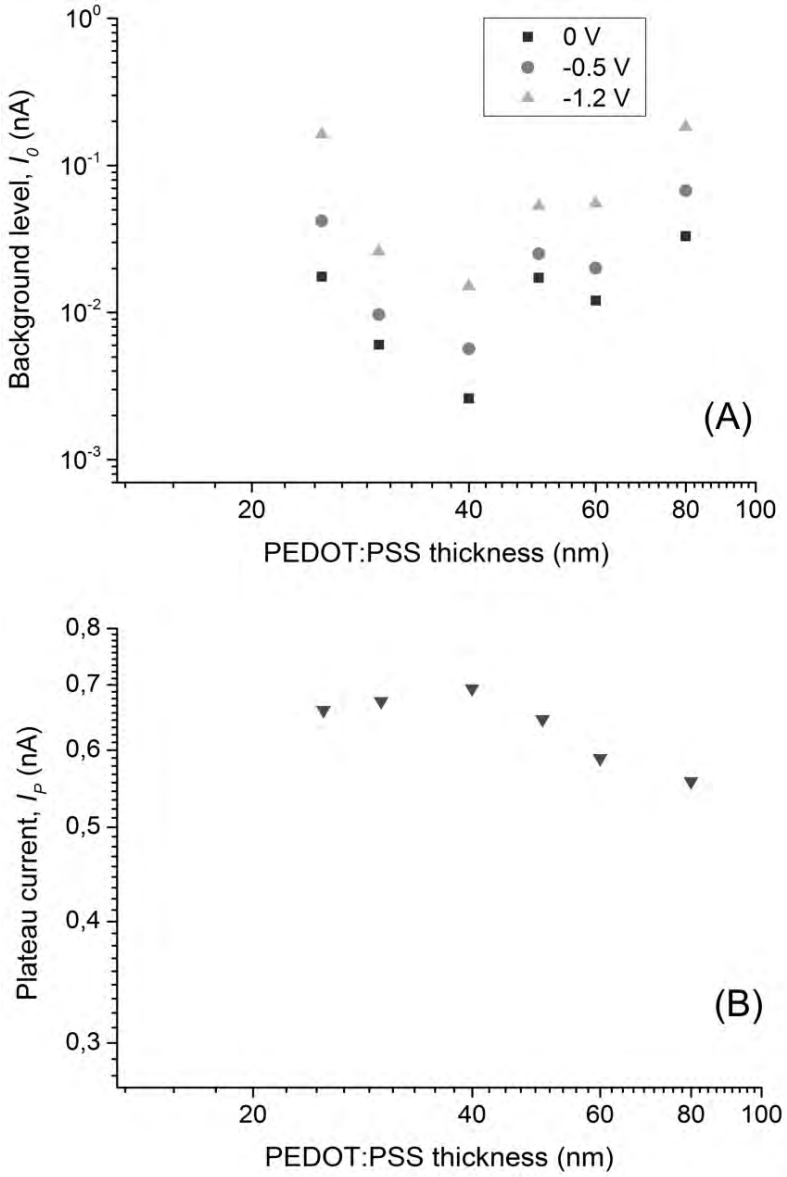

Fig. 7. Experimental optimisation of hole transport layer design. (a) Background current measured at different bias voltages as a function of PEDOT:PSS thickness. (b) Average photocurrent obtained from the plateau region of the transient CL response for different PEDOT:PSS thicknesses. CL detection was conducted with 10 ng/mL TSH.

2. *Optimisation of the CL assay*

Further tests of CL immunoassay optimisation were conducted with the optimised OPD comprising 120-nm-thick PCDTBT:$PC_{70}BM$ and 40-nm-thick PEDOT:PSS. Four concentrations of streptavidin-HRP conjugate ranging from 5 to 25 ng/mL were tested,

and the signal-to-noise ratio, defined as the current ratio of I_p to I_0, was used for the analysis. Enhanced signal-to-noise ratio was observed for a conjugate concentration of 15 ng/mL. This optimised concentration may have led to reduced shot noise in the detection system, which may be related to fluctuations in the photon flux density. This noise is important for systems that have been designed to detect low-magnitude photocurrents. Furthermore, the flow rate was optimised to 55 µL/min for the delivery of the luminol/enhancer and stable H_2O_2 solution into the microfluidic chip. This value was found to provide an ideal compromise between high photocurrent response and signal stability.

3. *Current-voltage response*

In this work, initial tests of quantitative CL immunoassay detection were conducted under the optimal conditions as described above. Fig. 8 shows the current-voltage curves due to the detection of the various TSH concentrations prepared in PBS. The photocurrent data were determined from the plateau region of the transient CL signal (see typical signal in Fig. 6) by applying a range of bias voltages to the PCDTBT:PC_{70}BM OPD. Upon incubation of the integrated opto-microfluidic device with TSH, the photocurrent changed remarkably with the bio-analyte concentration. The photocurrent resulting from the detection of 5 ng/mL TSH was ~100-fold higher than that measured for a non-analyte concentration.

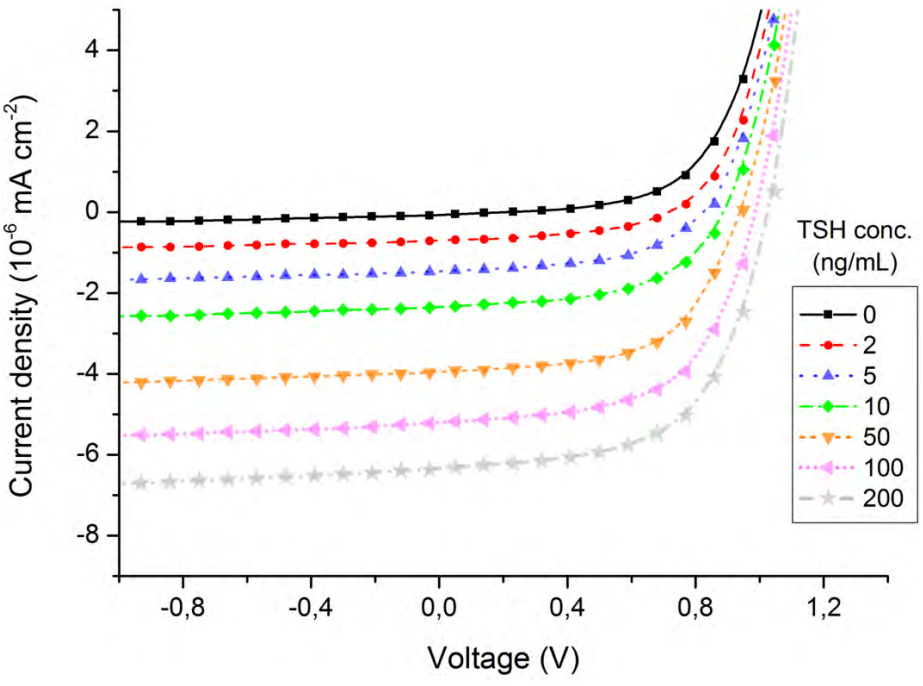

Fig. 8. Current-voltage profiles obtained with different concentrations of TSH targeted in the CL immunoassay.

2.1.2 Characterisation of OPD analytical performance (Article II)

Further demonstration of quantitative CL detection with the PCDTBT:$PC_{70}BM$ OPD pixel was conducted in Article II. The CL immunoassay targeted hydrocortisone or cortisol, a steroid hormone, which has drawn significant research attention for its potential use as a diagnostic marker of stress-related diseases [89]. The OPD pixel was coupled to Au-coated glass chips on which the cortisol immunoassays were performed. Artificial saliva, the preferred biofluid for in-field measurements of cortisol [90], was used to test the biosensing system, and its analytical performance for cortisol detection was thoroughly characterised in this study. The biosensor exhibited a linear response over four orders of magnitude, with a detection limit of ~tens of pg/mL and an analytical sensitivity of ~hundreds of pg/mL. Moreover, the biosensor showed high detection reproducibility and specificity. The results indicate that the PCDTBT:$PC_{70}BM$ OPD is promising for use in the POC detection of clinically relevant protein analytes.

Experiments

The analytical tests were performed according to the scheme described in Fig. 3(a). Reservoirs made of PDMS (400-µL volume) were attached between the Au-glass reaction chip and the OPD with the optimised ITO (100 nm)/PEDOT:PSS (40 nm)/PCDTBT:$PC_{70}BM$ (120 nm)/LiF/Al (~100 nm) architecture. The reservoirs were held in place on the reaction chip using a PMMA holder and contained all assay components which were confined to the surface opposite to the OPD. The reaction chip was pre-treated with 2% (w/v) thioctic acid, 1 mg/mL EDC and 0.8 mg/mL sulfo-NHS-biotin for immobilisation of 0.1 µg/mL of the cortisol capture antibody. After the Au surface was blocked with StartingBlock™ buffer, the chip was incubated with varying concentrations of cortisol for 30 min. This incubation was followed by the addition of 0.02 µg/mL HRP-labelled detection antibody and 150 µL aliquots of luminol/enhancer and stable H_2O_2 solution.

Results and discussion

Fig. 9 shows the calibration curve for the CL detection of cortisol in PBS buffer. The resultant photocurrent was normalised according to $\left[\left(I_p - I_0\right)/I_0\right]$ and plotted against the cortisol concentration. Here, I_0 was the background current corresponding to the negative control reaction chip/blocking buffer/capture antibody. To minimise the

background levels, the current measurements were performed by applying no bias voltage to the OPD, as indicated in Fig. 7(a) of Article I. The calibration plot revealed linearity for cortisol detection over the range of 0.1 to 180 ng/mL with a correlation coefficient of 0.994. The analytical sensitivity, determined from the slope of the linear region, was 642 pg/mL, while the detection limit was 65 pg/mL, as estimated from three times the standard deviation of five blank measurements.

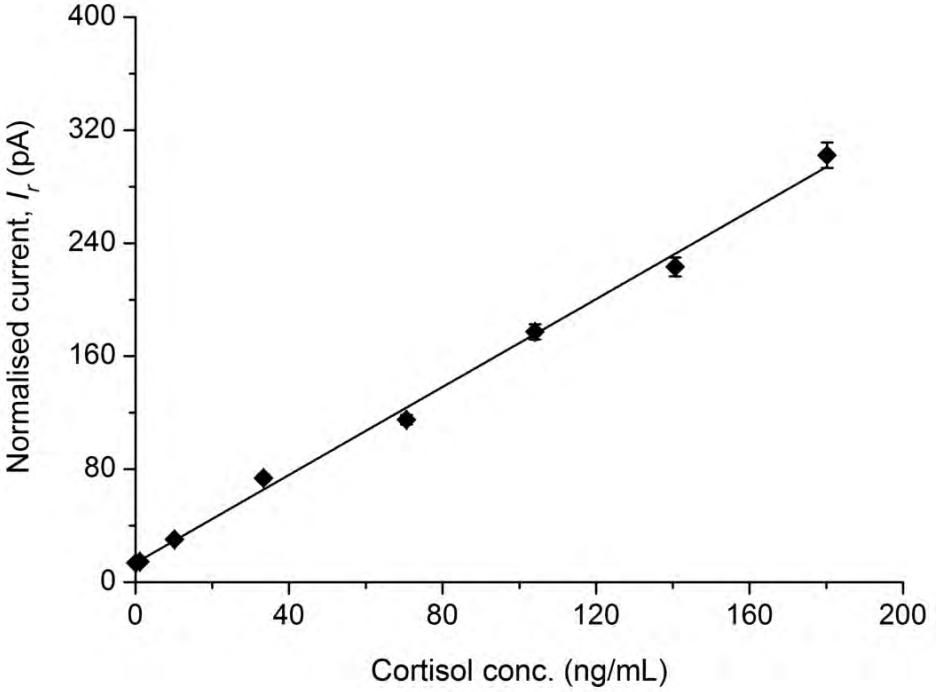

Fig. 9. Dose-response curve obtained from CL detection of cortisol in PBS samples. I_r represents the normalized photocurrent measured by the PCDTBT:$PC_{70}BM$ OPD.

The specificity of the developed cortisol biosensor was tested using various reagent blanks, 21-hydroprogesterone as a negative control and 20 ng/mL cortisol as a positive control. No significant interference from the blocking buffer, antibodies or luminol/H_2O_2 working solution on the photocurrent measurements was observed. Moreover, the variation of photocurrent for 21-hydroprogesterone, a glucocorticoid hormone that is highly similar to cortisol, was negligible compared with cortisol.

The developed biosensing system was further challenged with diluted samples of artificial saliva spiked with cortisol. Artificial saliva (pH 7.2) was prepared by dissolving 0.6 mg/mL Na_2HPO_4, 0.6 mg/mL anhydrous $CaCl_2$, 0.4 mg/mL KCl, 0.4 mg/mL NaCl, 4 mg/mL mucin and 4 mg/mL urea in deionised water according to the method described by Tlili *et al.* [89]. The photocurrent data obtained for the detection of

various cortisol concentrations in artificial saliva was normalised via $\left[\left(I_{\mathrm{p}}-I_0\right)/I_0\right]$ and plotted in a new calibration curve (Fig. 10).

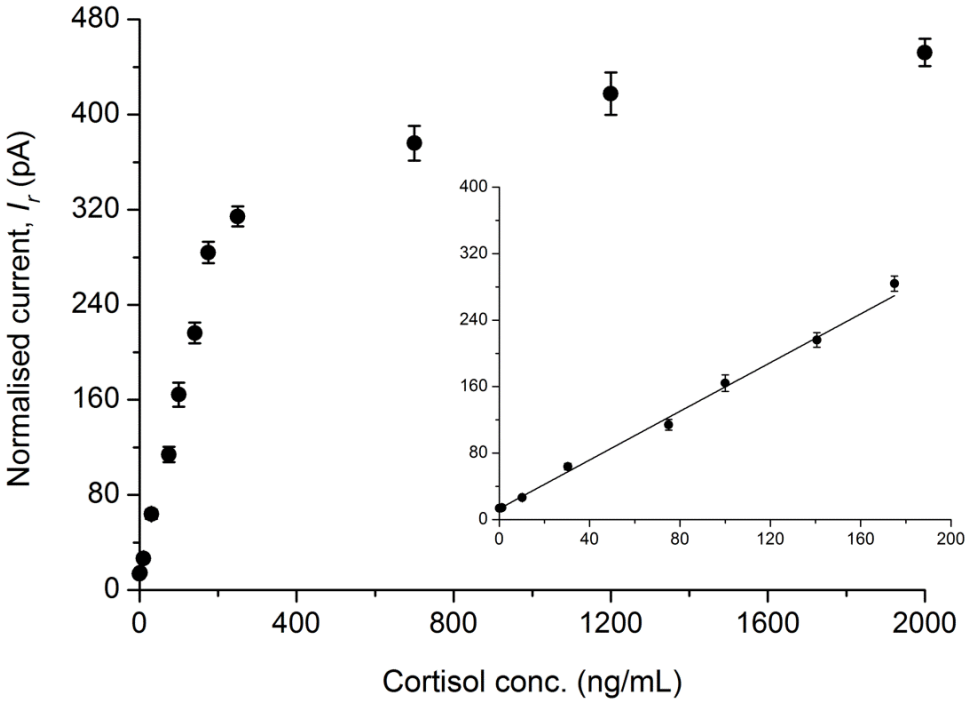

Fig. 10. Dose-response curve obtained from CL detection of cortisol in artificial saliva samples. Normalized photocurrent I_r measured by the PCDTBT:$PC_{70}BM$ OPD. The inset depicts the linear detection range.

The results of the analytical performance for detection in artificial saliva are summarised in Table 4. These data were compared with those obtained with a conventional ELISA method, whose CL readings were performed using a microplate reader.

The detection limit was more than three-fold better than that of the ELISA method and was below the 1 ng/mL lower limit of the cortisol reference range for healthy adults [91]. However, comparable analytical sensitivity was achieved by both detection methods. Compared with the results obtained for analysis PBS, the detection limit and sensitivity of the developed biosensor showed no significant variation with the background matrix. This result is in contrast to that of electrochemical-based sensors [90]. Furthermore, the intra- and inter-assay variability was less than 7% and 8%, respectively, indicating good detection reproducibility for the OPD-coupled CL biosensor.

	CL detection by OPD	**ELISA**
Detection range 10^3(pg/mL)	0.1 – 175	1 – 500
Analytical sensitivity (pg/mL)	685	628
Detection limit (pg/mL)	80	315
% Variability		
Intra-assay	3.3 – 6.7	4.1 – 12.3
Inter-assay	3.2 – 7.2	6.9 – 16.7
Total assay duration (h)	~6	~14
Biosensor miniaturisation	Yes	No

Table 4: Analytical performance of the developed CL biosensor with OPD based detection in comparison with ELISA method. Results are shown for cortisol detection in artificial saliva samples.

2.2 Multiplexed chemiluminescence detection

2.2.1 Microfluidic sensor integrating multiple OPDs (Article III)

Multiplexed CL detection of bio-analytes has been demonstrated using CCD cameras and a-Si:H photodiodes [57, 58]. However, OPDs have not yet been exploited in multiplexed optical biosensors. In this work, a multiplexed CL detection platform was developed by integrating a glass slide containing multiple PCDTBT:$PC_{70}BM$ OPDs with a hybrid PDMS-PMMA microfluidic chip. A unique characteristic of the developed platform is that its fabrication is compatible with mass production methods because of the use of simple spin-coating and injection moulding for the fabrication of the OPD pixels and PMMA chip. This microfluidic biosensor was applied to the detection of waterborne pathogens, using CL immunoassays performed on the PMMA chip. Both drinking water and surface water are vulnerable to *Escherichia coli*, *Legionella pneumophila* and rotavirus, among others [43, 92]. Thus, POC devices capable of performing multiplexed tests are ideal for the rapid detection of these pathogens in water. In addition to design demonstration, the characterisation of OPD analytical performance for individual pathogen detection is presented in Article III.

Design and experiments

The multiplexed opto-microfluidic biosensor is depicted in Fig. 11. The microfluidic channel layer is composed of a microchannel network connecting sixteen CL reaction chambers. The sample is loaded in the microfluidic chip through only one inlet. The fluid is then guided along two microchannels and enters the ~30 mm^3 volume chambers, where the CL immunoassays are performed on the transparent PMMA surfaces. Further, CL light is detected by a 16 mm^2 active area PCDTBT:$PC_{70}BM$ OPDs aligned below the chambers (Fig. 12). A PDMS lid was used to seal the PMMA chip. The hybrid system of PDMS and PMMA allows the realisation of microchannels with high conformity, enabling the complete filling of reagents within the channel network. Furthermore, large-area bonding of microfluidic chips, which is ideal for multiplexed detection devices, can be accomplished using the PDMS-PMMA interface [93].

The PMMA microfluidic chip was produced by an injection moulding method. The mould plate was cleaned with ethyl alcohol and pre-treated with oxygen plasma. The plate was then exposed to a 1% (v/v) solution of (3-aminopropyl)triethoxysilane (APTES) in deionised water, while the PDMS lid was treated with oxygen plasma. The APTES-modified PMMA was irreversibly bonded to the plasma activated PDMS at room temperature. This method of PMMA-PDMS bonding is highly stable and can withstand fluid flow pressures greater than 500 kPa [93]. The fluidic access holes for the inlet, air-bleeders, reservoir inlets and the outlet were punched through the PDMS, and the microfluidic setup was completed by attaching the PDMS to a glass slide (see Fig. 11 and Fig. 12). Further, the PMMA was attached to a second glass slide containing sixteen PCDTBT:$PC_{70}BM$ OPDs. The 100-nm thick ITO coating glass was patterned using HCl/HNO_3 wet etching to form sixteen anodes. This process was followed by spin coating a 40-nm-thick layer PEDOT:PSS and a 120 nm layer of PCDTBT:$PC_{70}BM$. Then, sixteen LiF/Al cathodes were thermally evaporated onto the polymer devices using a shadow mask.

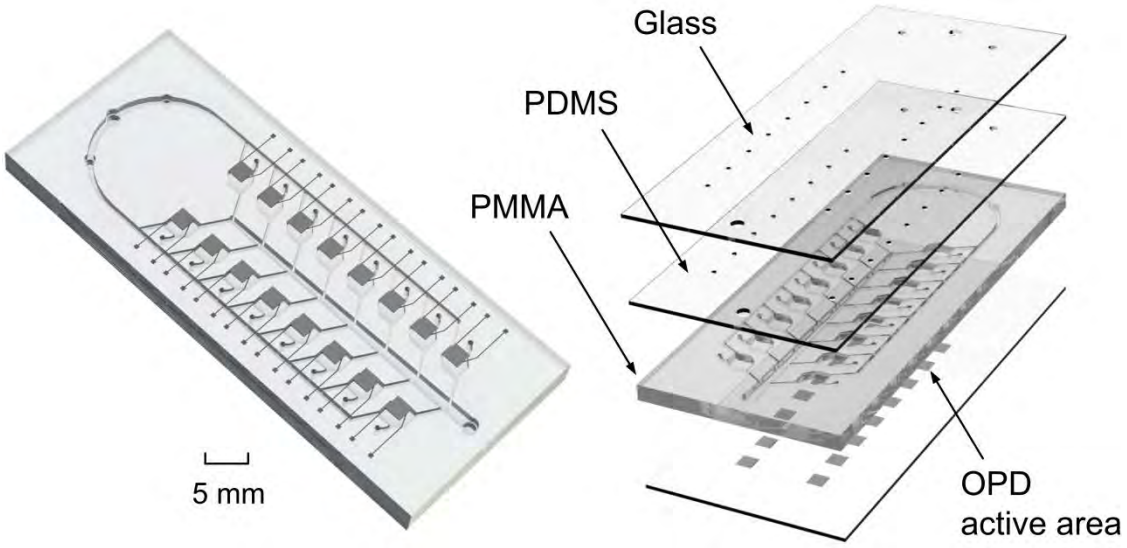

Fig. 11. Multiplexed opto-microfluidic device integrating a hybrid PDMS-PMMA chip and multiple PCDTBT:$PC_{70}BM$ OPD pixels prepared on a single glass chip.

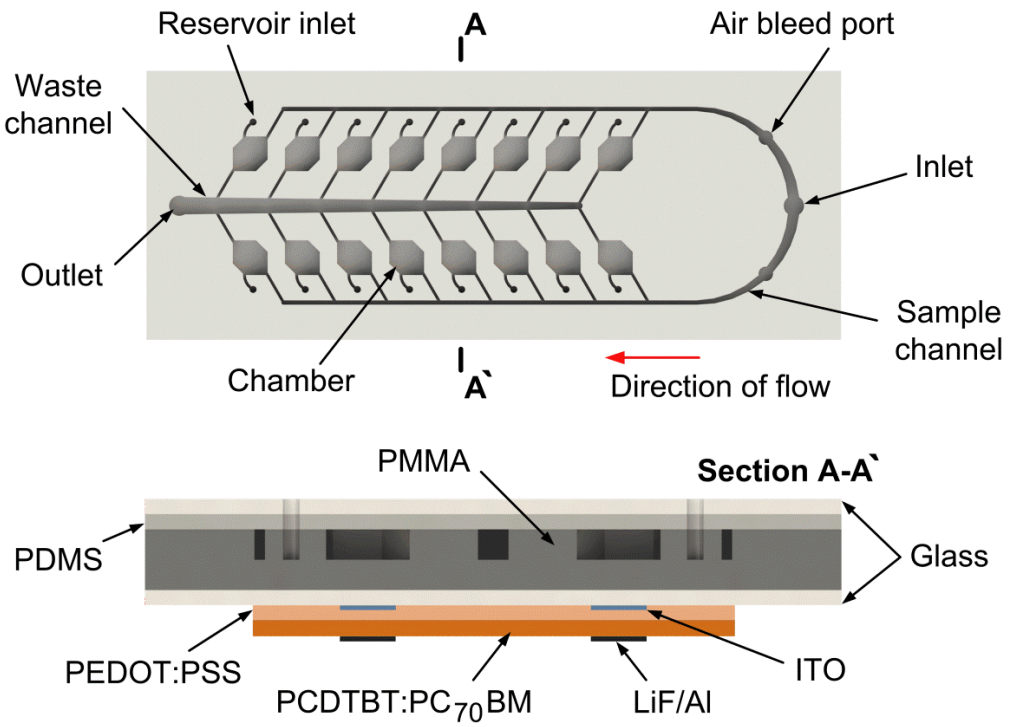

Fig. 12. Top view of the PMMA microfluidic chip, and cross-section view of the integrated opto-microfluidic device illustrating all device components (not to scale).

Results and discussion

Individual pathogen tests were performed to analyse the detection performance of the PMMA-integrated PCDTBT:$PC_{70}BM$ OPD pixel for *E. coli*, *L. pneumophila* and rotavirus, utilising a CL immunoassay scheme similar to that described in Article I. The

transient responses for the detection of various *E. coli* concentrations are shown in Fig. 13. The plateau regions of the CL signals were used to obtain calibration curves for each pathogen spiked in PBS samples. The average photocurrent between 3 and 7 min of the transient signals were plotted against the pathogen concentration. From the resultant calibration curves, it was found that the integrated PCDTBT:$PC_{70}BM$ OPD demonstrated good linearity for pathogen concentrations covering least 2 orders of magnitude ($R^2 > 0.99$). Moreover, the minimum pathogen concentration detected by the OPD was in the range of 10^5 cells/mL for *E. coli*, 10^6 cells/mL for *L. pneumophila* and 10^{-4} μg/mL for rotavirus. These detection limits corresponded to concentrations equivalent to three times the standard deviation of the background levels ($n = 5$) dividing by the slope of the linear region. The detection limit values for *E. coli* and *L. pneumophila* detection did not differ significantly from those obtained with previously reported CL immunoassay sensors [92, 94].

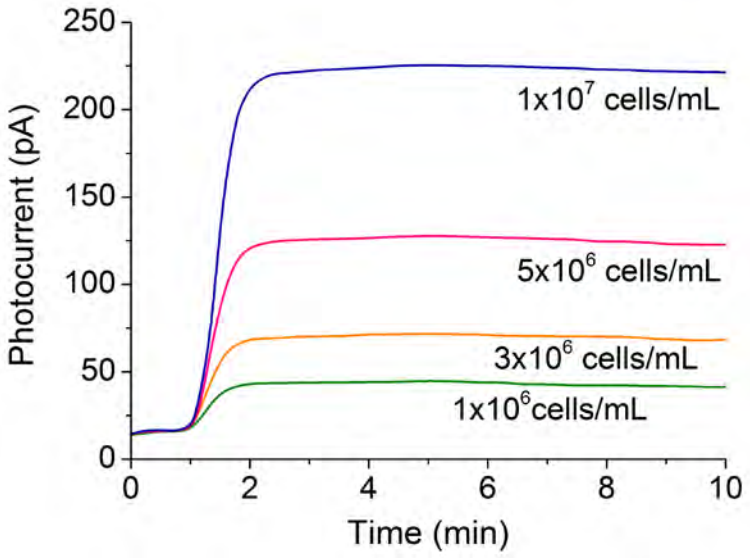

Fig. 13. CL detection of *E. coli* cells in the PMMA chamber using the integrated PCDTBT:$PC_{70}BM$ OPD pixel. The transient responses were measured by the OPD under short-circuit conditions.

2.2.2 Realisation of parallel CL detection (Article IV)

In this work, the multiplexed opto-microfluidic biosensor proposed in Article III was further used to demonstrate waterborne pathogen detection in parallel CL immunoassays. Three pathogens were combined in one water sample, and the feasibility of using the OPD-integrated PMMA microfluidic chip to simultaneously detect multiple bacteria and a virus was shown. Multiplexed detection was extended to drinking water and surface water samples. The realisation of parallel assay tests in less than 35 min was

demonstrated. Furthermore, the responsivity (R) and current-voltage (J-V) characteristics of the PCDTBT:$PC_{70}BM$ OPD were also characterised in Article IV.

Experiments

The experiments for parallel pathogen detection were conducted with the setup illustrated in Fig. 14. Heat-killed *E. coli* O157:H7 cells, heat-killed *Campylobacter jejuni* cells and inactivated adenovirus antigen were spiked in ultrapure water and targeted in three chambers of the opto-microfluidic biosensor shown in Fig. 12. The APTES-modified PMMA surface in chambers A to C, previously activated by 50 nM NHS and 200 mM EDC, was coated with pathogen specific monoclonal antibodies. No antibody was coated in chamber , which served as a negative control.

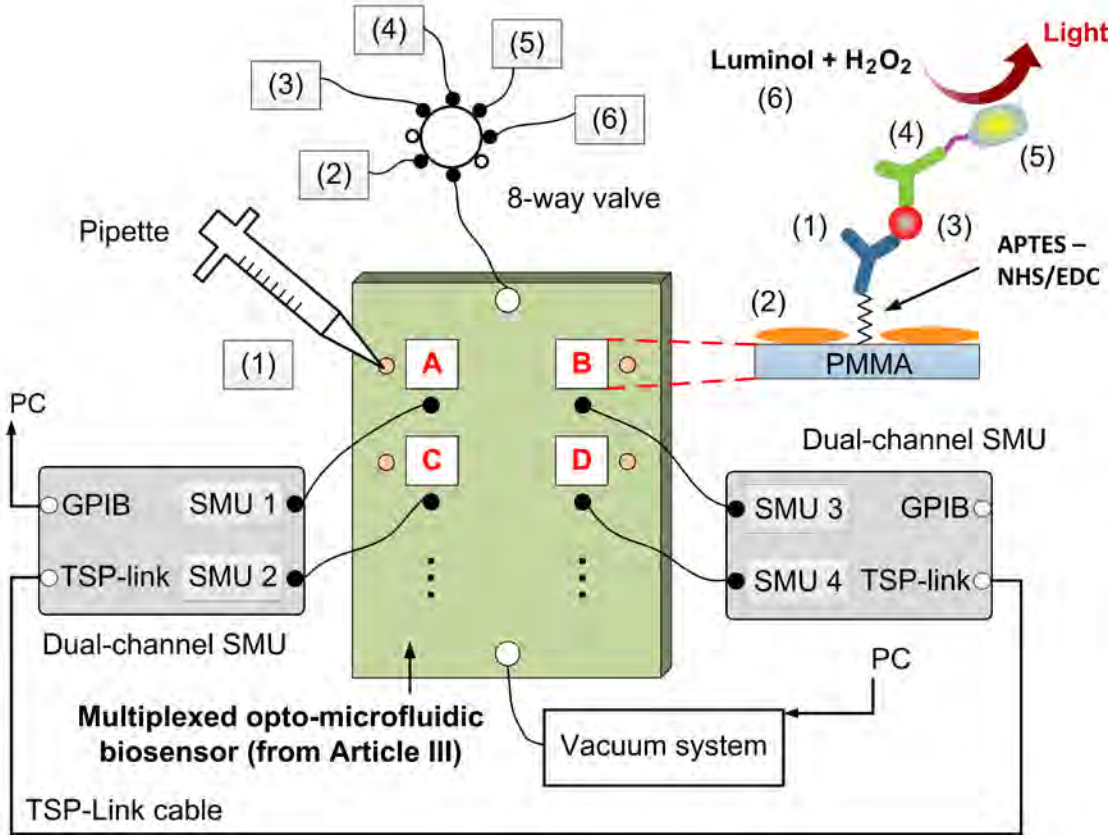

Fig. 14. Diagram of the complete setup used to demonstrate the multiplexed pathogen detection. Four detection zones (A to D, PMMA chamber + OPD) were monitored using two dual-channel SMUs, and parallel CL immunoassays were performed following the protocol: (1) monoclonal antibody; (2) blocking buffer; (3) sample; (4) biotinylated antibody; (5) streptavidin-HRP conjugate; (6) CL substrate.

The solutions of monoclonal antibody were added to the opto-microfluidic biosensor via the reservoir inlets, while the other assay components were flushed into the chip

through the main inlet (see Fig. 14). The pathogen-spiked samples (180 μL) were loaded into chip after the chamber surfaces were blocked with StartingBlock™ buffer. Sample addition was followed by the addition of 1 μg/mL biotinylated antibody and 0.015 μg/mL streptavidin-HRP conjugate. The CL signals obtained after the addition of 180 μL of a solution of luminol and H_2O_2 were measured by four PCDTBT:PC_{70}BM OPDs placed below chambers A through D. Parallel measurements of photocurrent were ensured by two Keithley 2600A SMUs connected to the four OPDs. These SMUs are dual-channel instruments and can be interconnected via an embedded Test Script Processor (TSP) provided by the manufacturer.

Results and discussion

The optoelectronic performance of the OPD in terms of *J-V* [Fig. 15(a)] and *R* [Fig. 15(b)] was analysed prior to its integration in the PMMA-PDMS hybrid chip. The *J-V* curves were obtained by measuring the OPD photocurrent in the dark and under laser diode illumination. These curves present an asymmetric behaviour which indicates an effective collection of photoinduced charge carriers [94]. The dark current density (J_{dark}) measured by applying no bias was 2.88×10^{-9} mA/cm^2. A 405 nm laser diode was used for the measurements because of its proximity to the 425 nm wavelength emitted by the CL of the HRP and luminol/H_2O_2 system.

R of the PCDTBT:PC_{70}BM OPD was determined in terms of EQE following the relation [94]:

$$R = \frac{\eta \lambda q}{hc} \tag{2}$$

where η represents the EQE estimated by eq. (1) in Article I, λ is the incident light wavelength, q denotes the elementary charge constant, h is the Planck constant and c is the light velocity. For 425 nm, *R* was 0.21 A/W, which contrasts the response of 0.10 A/W, obtained at same wavelength by an OPD pixel prepared from a P3HT:PC_{60}BM blend heterojunction [62]. Moreover, *R* and J_{dark} were analysed for ten of the sixteen PCDTBT:PC_{70}BM pixels fabricated in the multiplexed opto-microfluidic device. The maximum difference between pixels was 8% and 29% for *R* and J_{dark}, respectively.

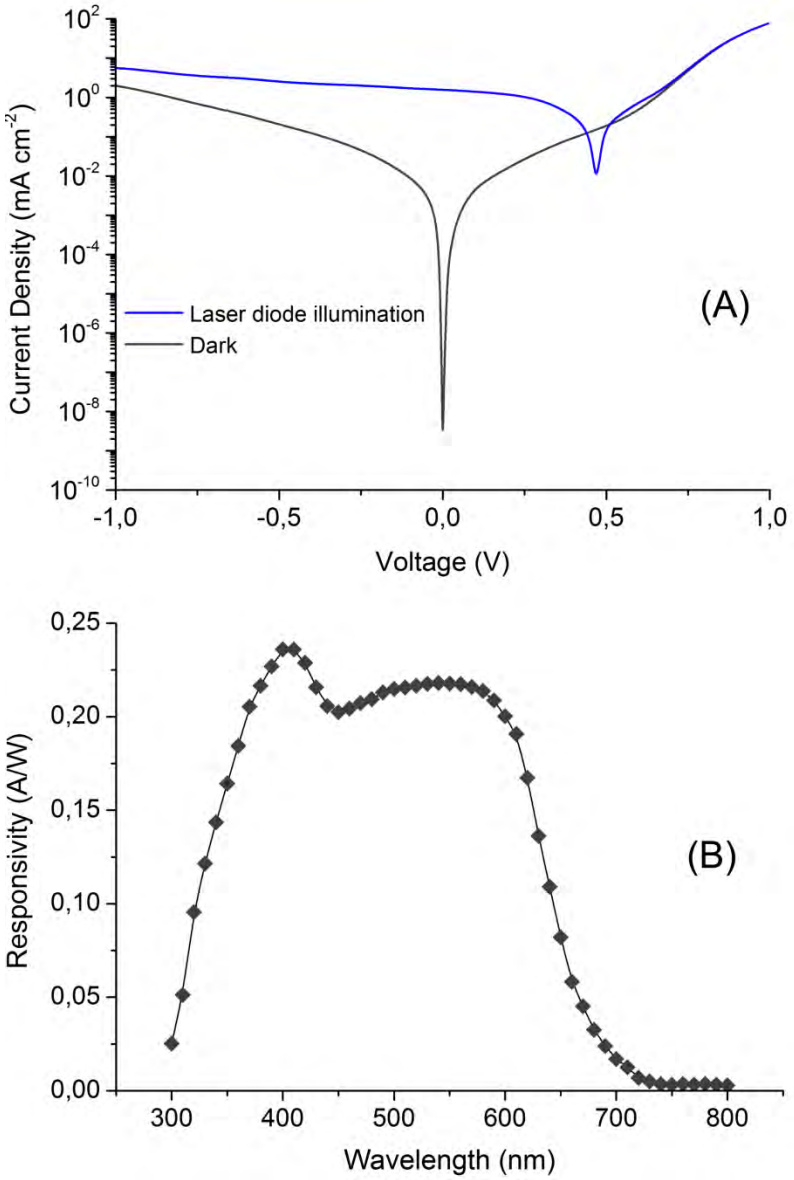

Fig. 15. Optoelectronic performance of the PCDTBT:$PC_{70}BM$ OPD pixel before microfluidic integration. (a) *J-V* curves for the pixel in dark and under laser diode illumination. (b) Photosensitivity spectral response.

The characterisation of OPD optoelectronic performance was followed by testing the antibody-antigen recognition in the four chambers, A through D, of the opto-microfluidic device. For the first multiplexed detection experiments, individual samples consisting of 6.5×10^6 cells/mL *E. coli*, 3×10^7 cells/mL *C. jejuni*, and 5×10^{-7} mg/mL adenovirus were separately incubated within the four chambers. The CL signals were recorded in parallel as illustrated in Fig. 14. The photocurrent results shown in Fig. 16 indicated that the monoclonal antibodies immobilised on the PMMA surface were highly specific for their corresponding targets.

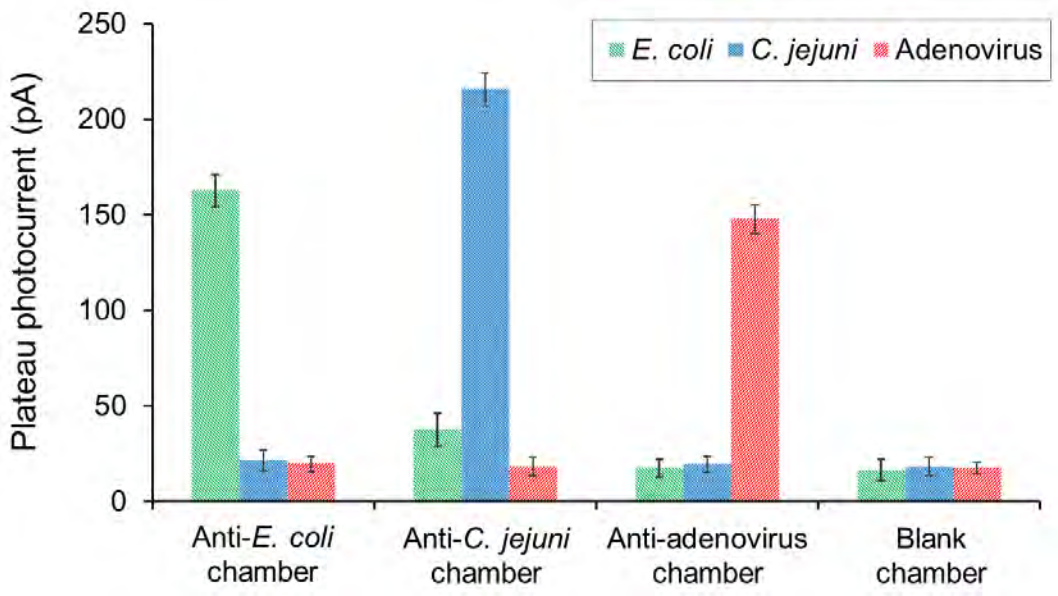

Fig. 16. Antibody-antigen specificity tests using single samples of *E. coli*, *C. jejuni* and adenovirus. Detection of each pathogen was tested in the four chambers A-D (Fig. 14), and the photocurrent taken from the plateau of CL signal was measured in parallel.

The absence of cross-reactivity between antibodies and nonspecific pathogens enables the parallel detection of bio-analytes in one sample. Thus, the multiplexed opto-microfluidic device was further challenged with samples containing a mixture of *E. coli*, *C. jejuni* and adenovirus. The results of the parallel detection tests shown in Fig. 17 demonstrated the device's ability to distinguish pathogen concentration in multiplexed conditions at high sensitivity. However, it is possible that varying amounts of pathogen could reach the target chamber because the fluid flow separates after sample loading (see design in Fig. 12). This variation might explain the different plateau photocurrent values recorded for the same *E. coli* concentration spiked into two mixture samples (Fig. 17).

The analysis time per parallel detection test was approximately 35 min, including sample loading, incubation and photocurrent measurement. A test analysis time of 30 min may be sufficient in POC settings [19], while conventional detection methods typically require at least 1-2 h to obtain an accurate result [32]. Moreover, although other CL detection systems showed an overall analysis time of 18 min [31], the parallel detection was achieved using a CCD camera that was not integrated into the microfluidic chip.

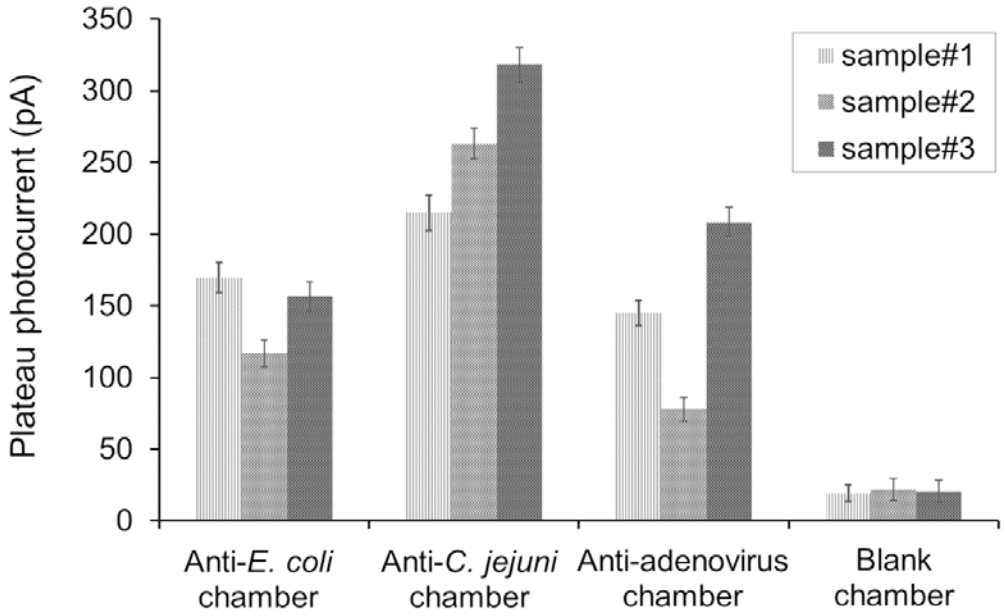

Fig. 17. Parallel detection tests using three samples of a mixture of *E. coli*, *C. jejuni* and adenovirus. Sample#1 contained 6.5 × 10^6 cells/mL *E. coli*, 3 × 10^7 cells/mL *C. jejuni* and 5 × 10^{-7} mg/mL adenovirus. Sample#2 was made of 5 × 10^6 cells/mL *E. coli*, 5 × 10^7 cells/mL *C. jejuni* and 1 × 10^{-7} mg/mL adenovirus. Sample#3 contained 6.5 × 10^6 cells/mL *E. coli*, 1 × 10^8 cells/mL *C. jejuni* and 5 × 10^{-6} mg/mL adenovirus.

Although the study of multiplexed CL detection was limited to three pathogens in Article IV, the developed opto-microfluidic device has potential for analysing up to sixteen bio-analytes by immobilising different specific antibodies onto the sixteen chambers. Additionally, feasibility for multiplexed detection was further demonstrated by testing real water samples spiked with *E. coli* and *C. jejuni*. Mixture samples of both bacteria were prepared from filtered drinking water and surface water, and parallel detection was conducted in chambers A and B. The results of analyte recovery showed that the opto-microfluidic device detected 79 to 107% of the spiked organisms. To determine the recovery, the device was previously calibrated using both *E. coli* and *C. jejuni* individually spiked in the water samples.

2.3 Methods of enhancing opto-microfluidic detection sensitivity

2.3.1 Gold nanoparticle enhanced CL immunosensor (Article V)

The detection performance of opto-microfluidic devices can be further improved by developing photodetectors with higher sensitivity and/or enhancing the detection

sensitivity of the bio-analyte assays. In Article I, the performance of the PCDTBT:$PC_{70}BM$ OPD was improved by optimising the thickness of the photoactive layer and the hole transport layer. Here, the CL immunoassay was enhanced by employing commercially available gold nanoparticles (AuNPs) as enhancers for the HRP-luminol H_2O_2 CL reactions [95]. The AuNPs were incorporated into a PDMS-glass hybrid microfluidic chip, and CL detection of 17-β estradiol (E2), an important endocrine disrupting compound [41], was conducted by the PCDTBT:$PC_{70}BM$ OPD. The resultant opto-microfluidic device was subsequently demonstrated to be useful for detection in complex media, including natural water and serum. In addition, the remarkable stability and specific detectivity (D^*) of the PCDTBT:$PC_{70}BM$ OPD was characterised. The motivation for this study was to realise a miniaturised ultrasensitive approach for simple inexpensive POC systems.

Experiments

The integrated AuNP-CL opto-microfluidic device is shown in Fig. 18(a). For device fabrication, a glass slide with immobilised AuNPs is bonded to a PDMS microchannel layer by simple oxygen plasma treatment. The device is then completed by the attachment of a second glass slide containing the PCDTBT:$PC_{70}BM$ OPD pixel to the PDMS chip.

The PDMS microchannel consisted of nine parallel channel segments connecting one inlet and one outlet. The channels segments, measuring 280 μm in width and 80 μm in depth, were covered by separate AuNP lines. These lines of nanoparticles were previously assembled on the cover glass using 280-μm-wide trenches patterned onto an auxiliary PDMS chip. A reversible bonding method was used to attach the auxiliary PDMS to the cover glass, thereby permitting the easy demounting of the parts before permanent attachment of the cover glass to the PDMS microchannel layer. The area (4×4 mm^2) occupied by the AuNP lines on the glass matched the active area of the integrated OPD [Fig 18(a)]. The procedure of AuNP immobilisation involved modification of the AuNP surface with carboxyl groups (using dithiodipropionic acid) and modification of the glass surface with amine groups (using APTES). Covalent binding was achieved via carboxylamine coupling reactions [96]. Unreacted carboxyl groups on the AuNP surface were then used to conjugate biotinylated IgG antibody using NeutrAvidin [Fig 18(b)].

The competitive binding CL immunoassay principle was used to detect the E2 antigen along the multiple AuNP lines within the PDMS microchannel. Briefly, in this assay, the target E2 competes with added E2-HRP conjugate for binding to the antibody-modified AuNPs. After washing out unbound material from the integrated device, the luminol-H_2O_2 substrate is added to react with HRP which catalyses the luminescent reaction. The intensity of 425 nm light generated is then inversely proportional to the E2 concentration.

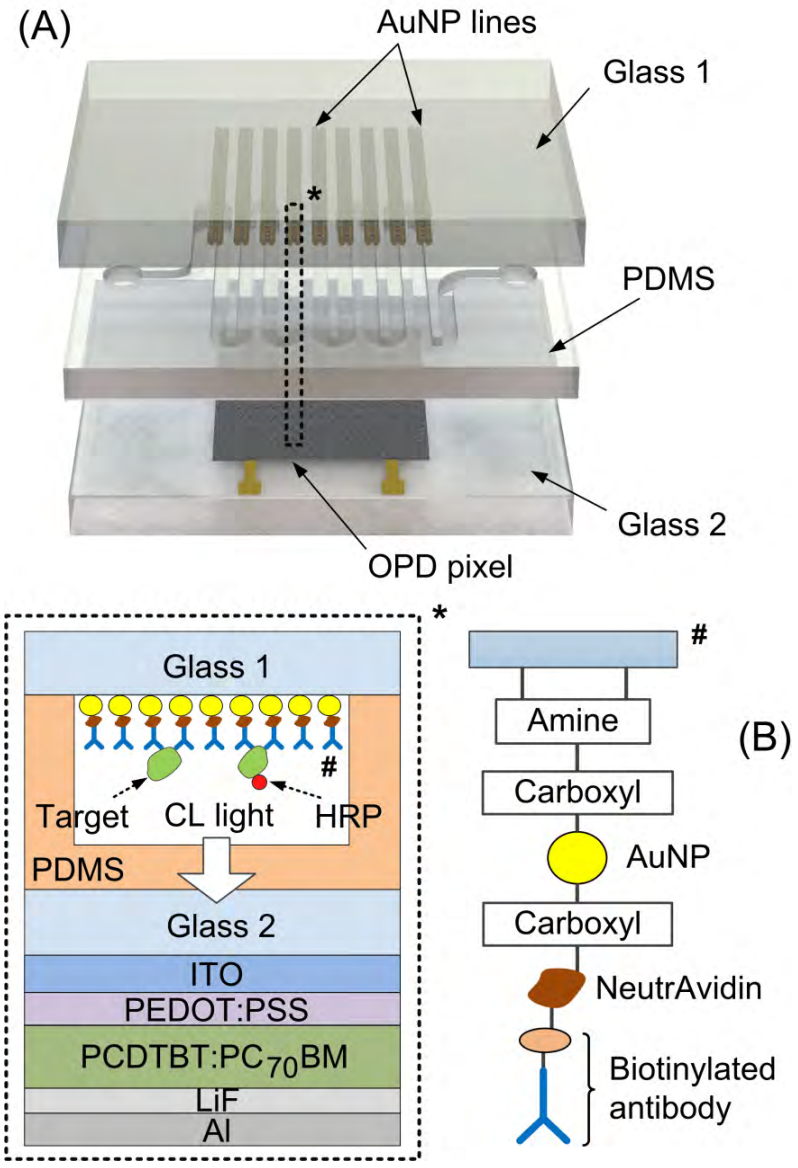

Fig. 18. Microfluidic AuNP optical immunosensor. (a) Microfluidic integration of the AuNP glass slide, PDMS microchannel chip and PCDTBT:PC_{70}BM OPD pixel. (b) Procedure of AuNP and biomolecule immobilisation onto a glass slide and cross-section scheme of the detection zone showing the AuNP-enhanced CL competitive immunoassay. Device layers are not to scale.

Results and discussion

CL was measured using the OPD architecture of ITO/PEDOT:PSS/PCDTBT:$PC_{70}BM$/LiF/Al, as previously described in Article I. However, in this study, the photocurrent measurements were performed without applying a protective encapsulation to the OPD. PCDTBT is remarkably stable against oxidation due to its deep highest occupied molecular orbital level [81]. Furthermore, the high short-circuit photocurrent and low dark current acknowledged for the PCDTBT:$PC_{70}BM$ OPD [82] may result in high D^*.

For the bio-assay conditions developed in this work, it was expected that D^* of the OPD [97] (commonly expressed by $D^* = (A\Delta f)^{1/2} R/i_n$, where A is the effective area of the OPD, Δf is the electrical bandwidth, R is the responsivity, and i_n is the noise current) is primarily limited by the shot noise from the dark current. Thus, D^* can simply be calculated from the measured photocurrent (J_{ph}) and dark current (J_d) as follows:

$$D^* = \frac{R}{(2qJ_d)^{1/2}} = \frac{(J_{ph}/I_{light})}{(2qJ_d)^{1/2}}, \quad (3)$$

where I_{light} is the incident light intensity and q is the elementary charge constant (1.6×10^{-19} Coulombs). At zero bias, the calculated D^* was 9.2×10^{11} Jones for the PCDTBT:$PC_{70}BM$ OPD under LED illumination at 428 nm peak wavelength with 0.22 mW/cm^2 light intensity. A D^* result of $\sim 4 \times 10^{12}$ Jones is typically obtained by Si photodetectors [97]. An enhanced D^* of an OPD leads to a reduced noise equivalent power (NEP) level as demonstrated by

$$\mathrm{NEP} = \frac{(A\Delta f)^{1/2}}{D^*}, \quad (4)$$

and an improved NEP means an enhanced signal-to-background-current ratio (S/B).

The S/B ratio was determined for a number of AuNP-CL assay tests. For these assays, E2-spiked PBS samples were incubated within the PDMS microchannel after the microchannel was treated with StartingBlock™ blocking buffer. The OPD photocurrent was measured immediately after 5 min of exposure to the luminol/H_2O_2 substrate. The photocurrent obtained with 0 ng/mL E2-HRP conjugate was defined as the background

for S/B determination. The first results for S/B showed that the OPD response varied with the size of the AuNPs (Fig. 19). The decreased response for AuNPs with a diameter < 60 nm was likely due to absorption of the CL emission by the SPR phenomenon on the Au particles [98]. The wavelength of SPR related absorption is red shifted with increasing AuNP size, according to the manufacturer's information. Furthermore, the decrease in AuNP surface area may explain the reduced S/B for 100 nm particles, and no significant improvement in the OPD response was observed for a microchannel immobilising both 60 and 10 nm AuNPs.

The calibration curve for E2 detection with the 60 nm AuNPs is shown in Fig. 20. This curve was normalised by subtracting the photocurrent measured for a known E2 concentration from that obtained for the control sample containing only E2-HRP conjugate. The resultant curve of photocurrent variation (ΔS) was fitted to a three-parameter logarithmic equation. Based on the logarithmic fit, the detection limit was 2.5 pg/mL, which is in contrast to the 70 pg/mL obtained by CL immunoassays that employ no AuNPs (Fig. 20). Furthermore, the lowest limit of previously reported CL immunosensors employing other OPDs was 500 pg/ml [99].

The unique sensitivity to E2 detection was accompanied by rapid assay development. A run cycle of the AuNP-CL assay would take ~20 min, including sample incubation and CL signal detection.

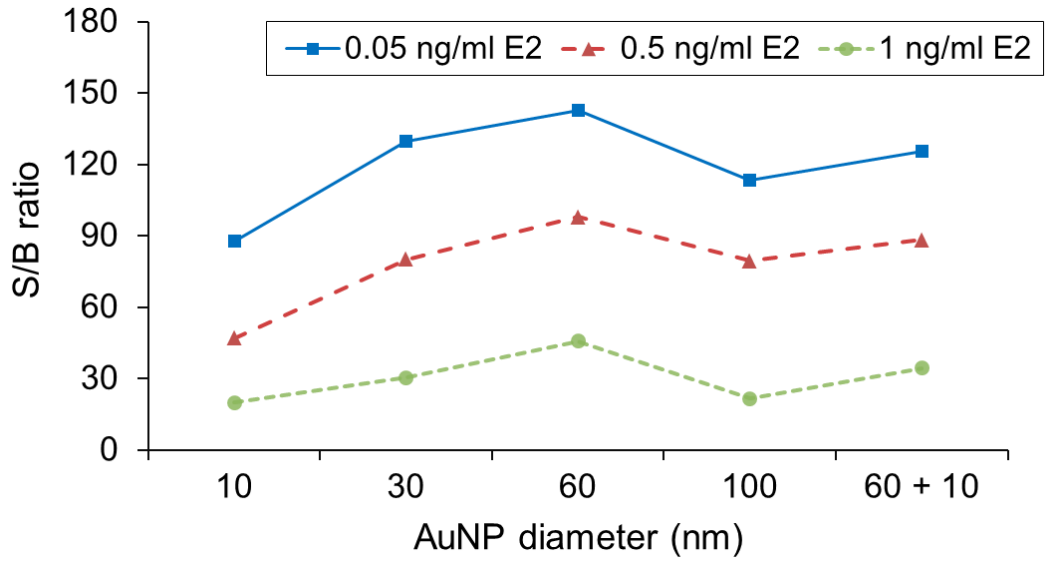

Fig. 19. Effect of AuNP diameter on measured signal-to-background current ratio (S/B) for the detection of E2 antigen in PBS samples using the AuNP-enhanced CL competition immunoassay.

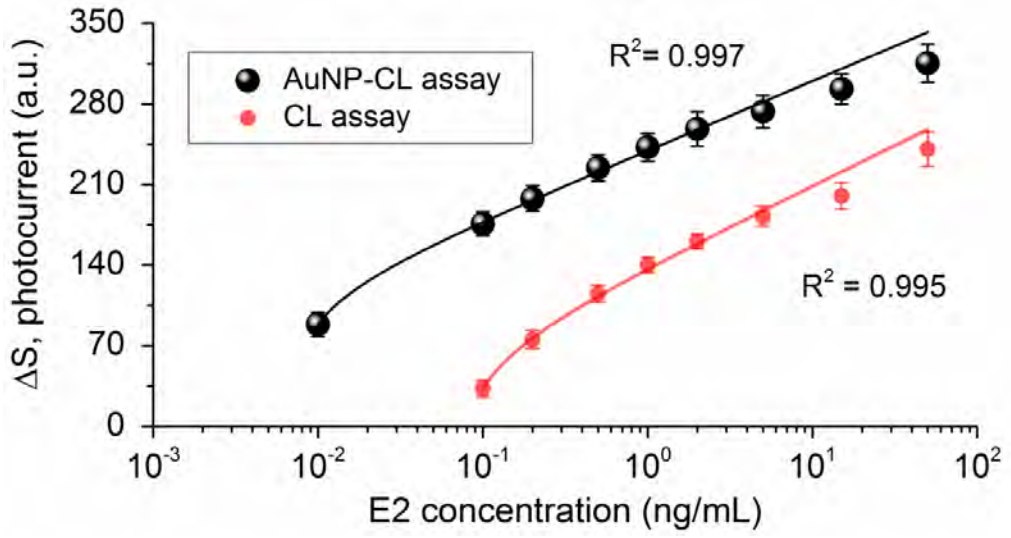

Fig. 20. Calibration plots for the E2 antigen obtained by performing CL immunoassays and AuNP-enhanced CL immunoassays.

The stability of the sensor response is relevant to single-use disposable POC devices because of the possibility for the long-term storage of these devices. Thus, the OPD-integrated AuNP-CL opto-microfluidic device was tested with E2 every three days, and the device was stored under ambient conditions between each test. After 15 days, the photocurrent response of a PCDTBT:$PC_{70}BM$ OPD decreased by only 25% of its initial value, presumably due to a small decrease in the charge mobilities of PCDTBT [81]. Additional tests conducted in this work to detect E2 in blood serum and filtered water indicated the potential of the AuNP-enhanced CL immunosensor for bio-analyte detection in various complex matrices.

2.3.2 Particle refining filters with enhanced recovery performance (Article VI)

Detection sensitivity can also be enhanced by preconcentration of the target bio-analyte before performing the optical detection. Preconcentration involves the substantial reduction of the sample volume while retaining the number of analytes, thus leading to a significant decrease in the smallest detectable concentration [100]. Preconcentration of 10-100 L water samples to a few mL is an indispensable step for the detection of hundreds or even tens of bacterial, viral and protozoan organisms [65]. Here, the recovery of two protozoan organisms, *Crytosporidium parvum* and *Giardia lamblia,* from large-volume environmental water samples is demonstrated using particle refining filters that were developed based on the counter-flow microfiltration principle. This

filtration principle was performed using the microconcentrator (μC) device depicted in Fig. 21.

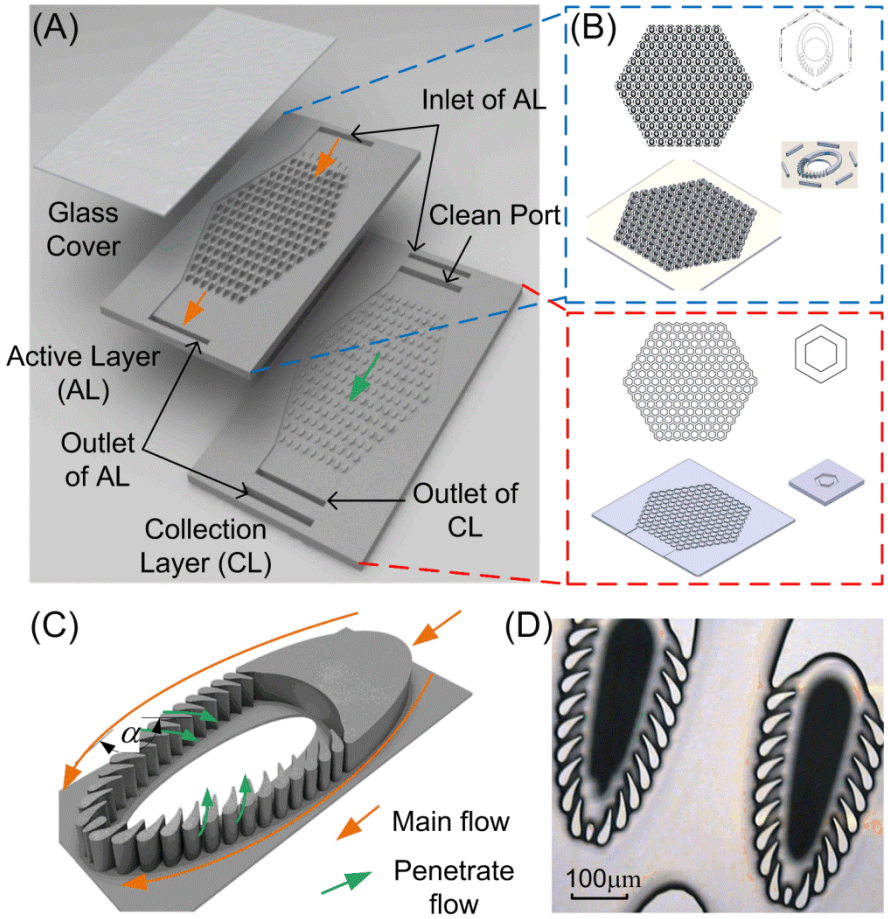

Fig. 21. (a) Microconcentrator with the three layers, glass covering layer, active layer and collection layer. Water sample is loaded into the active layer with the CFR cells, in which the particles are separated and concentrated. Filtrates are flushed out via the collection layer. (b) Honeycomb-like arrangement for both active layer and collection layer. (c) 3D model and (d) Micrograph of the CFR cell.

A detailed description of the design and fabrication of the μC can be found elsewhere [77]. Briefly, the μC mainly comprises two filtration layers, the active layer with counter-flow recovery (CFR) cells, and the collection layer [see Fig. 21(a)]. Continuous-flow concentration is conducted by the active layer where the CFR cells are arranged in a compact honeycomb-like structure [Fig. 21(b)]. The concentrate is guided via a fluid channel network generated between the cells, while the filtrate is discharged from the active layer to the collection layer, which consists of solid hexagonal micro-pillars that are similarly arranged with a honeycomb-like profile. Fig. 21(c) and 21(d) show the profile of one CFR cell. It includes a hollow centre as the outlet port for the filtrate comprising a barrier section with streamlined turbine blade-like micro-pillars.

Micro-sized gaps are set between each pair of adjacent pillars. According to the cell profile, the counter-flow principle is defined by the obtuse angle α between the local flow through the gaps and the main flow. Thus, when the main flow containing water particles passes around the cell, the larger particles are entrained by the main flow and pushed away from the gap entrances due to microfluidic hydrodynamics [101], while the smaller particles remain near the surface of the cell and enter the gaps. The particles larger than the gap size are separated from the smaller ones, which are guided to the filtrate flow.

2.3.2.1 Bio-analyte recovery by a multi-unit filtration system

The counter-flow μC was used as the basic unit of the filtration system developed in Article VI. This filtration system was developed by incorporating multiple μC units to achieve high concentrating ratios (10 to 100 L concentrated to < 200 mL) at short processing times (> 1 L/min) without recirculation. Using *C. parvum* oocysts and *G. lamblia* cysts at environmentally realistic concentrations spiked into real surface water samples, the filtration system showed recovery efficiencies above 80% which was in contrast to the recoveries of < 55% achieved by hollow fibre cross-flow filters [64, 102]. Moreover, no significant clogging failure was encountered in the filtration system while processing the surface water samples. The current lack of non-clogging and high-efficiency methods for the recovery of *C. parvum* and *G. lamblia* strongly limits the sensitivity of optical detection for these protozoan organisms in environmental water [103, 104].

Experiments

The filtration system was constructed with two water-particle separation or refining levels – L1 and L2 (see Fig. 22). Both refining levels consisted of μC units arranged in series, where the concentrate outlet of a μC unit was connected to the inlet of an adjacent unit. The filtrate outlet of each L1 unit served as the inlet of the corresponding unit in L2. The target protozoan organisms are recovered in L2, and non-targeted particles present in the surface water are collected in L1. Thus, based on this principle, the L2 units were designed with a gap of 3 μm to recover *C. parvum* oocysts (size 3.5–6 μm), while the L1 units were designed with a gap of 7 μm. To recover *G. lamblia* cysts (8–13 μm in diameter), 7 μm gap concentrators were used as the L2 units, and a gap of

14 μm was set for the L1 units. With the two system designs particulates > 14 μm and particulates > 7 μm can be separated from the cysts and oocysts, respectively.

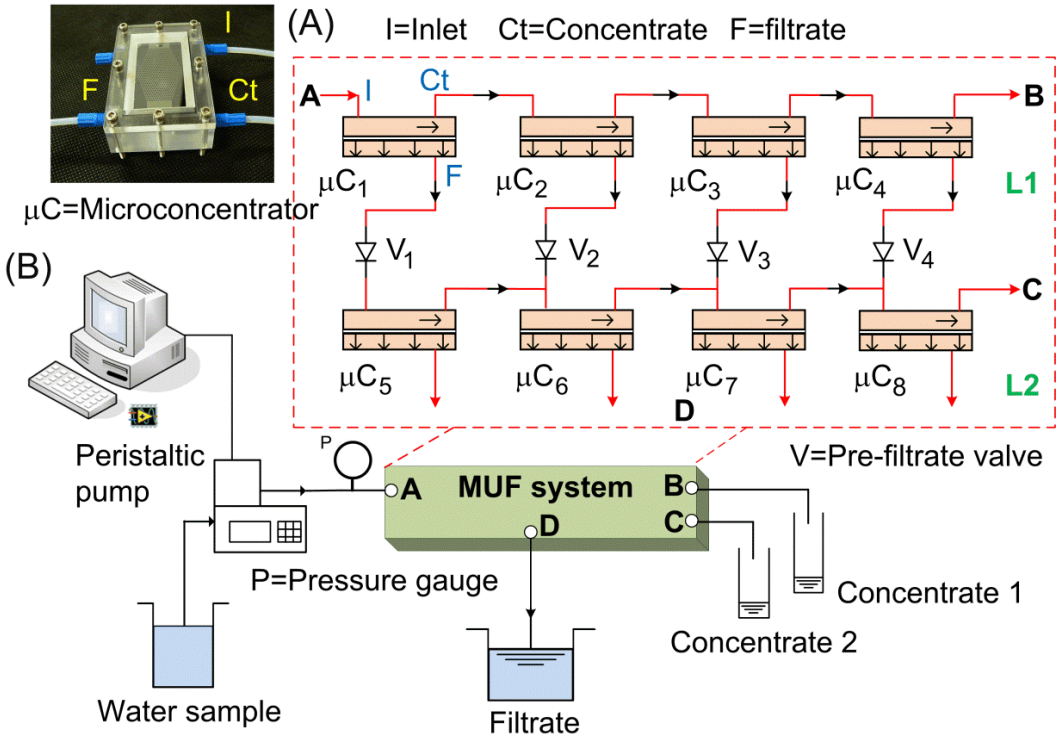

Fig. 22. (a) Multi-unit filtration (MUF) system. Four μC units per refining level (L1 and L2) are used for filtration of 10-L samples. When the water sample is driven into the system, the larger particles are concentrated in the μC units of L1 whereas the smaller one enter the units of L2. (b) Experimental setup. Port A and D is the inlet and filtrate outlet of the system, respectively. Port B and C are the concentrate outlets.

A unique characteristic of this system is that the number of μC units (N) per refining level can be varied to adjust the concentrating ratio for the final concentrate in L1 and L2. These concentrating ratios are determined by the ratio of the volumetric flow at the concentrate outlet of L1 (Q_{fin1}) and L2 (Q_{fin2}) to the volumetric flow rate at the main inlet (Q_{in}) as follows:

$$\frac{Q_{\text{fin1}}}{Q_{\text{fin2}}} = \frac{1}{\left(R_{\text{ref1}}+1\right)^{N}}, \tag{5}$$

$$\frac{Q_{\text{fin2}}}{Q_{\text{in}}} = \sum_{n=1}^{N} \frac{R_{\text{ref1}}}{\left(R_{\text{ref1}}+1\right)^{n}\left(R_{\text{ref2}}+1\right)^{N-n+1}}, \tag{6}$$

where R_{ref1} and R_{ref2} are the inherent concentrating factors of each L1 unit and L2 unit.

The μC units were connected together using commercial polymer tubing, and each μC was fabricated in silicon by use of inductively coupled plasma deep reactive-ion etching. Both the active and collection layer of the μC were arranged in two Si wafers that were combined by Si-Au-Si thermal bonding. For sealing, a Pyrex 7740 glass wafer was added to the aforementioned layers by anodic bonding. Further, the bonded μC chip was incorporated into a packaging device comprising a substrate with the fluid channels for connecting the inlet and outlets of the μC unit (Fig. 22). The μC is also amenable to mass production using micro-injection moulding of PMMA or a cyclic olefin copolymer.

Water concentration was performed by pumping the oocyst and cyst spiked surface water into the multi-unit filtration system via the inlet of the first μC (port A in Fig. 22). Water samples were combined with 0.5-1.7 L solution containing 0.1% Tween 80 and 0.001% antifoaming agent prior to filtration. The final concentrates (16-45 mL of concentrate 1 and 60-190 mL of concentrate 2) were collected from the outflow ports B and C, and the filtration system was flushed with pure water. The concentrate content was centrifuged at 1100 × g for 15 min, and the resultant pellet was subjected to IMS using commercially available immunomagnetic beads. The purified sample was then stained with fluorescein isothiocyanate conjugated antibodies and 4′,6′-diamidino-2-phenylindole dihydrochloride hydrate to visualise the *C. parvum* oocysts and *G. lamblia* cysts via immunofluorescence microscopy (IFM). The recovery efficiency was calculated by dividing the number of oocysts and cysts enumerated after the IMS procedure by the total number of organisms spiked in the initial sample.

Results and discussion

The inherent concentrating factors R_{ref1} and R_{ref2} of the 3 μm-, 7 μm-, and 14 μm-gap μC units were experimentally determined before the recovery tests were conducted. The units were individually tested with 10 L of lake water over a wide range of flow rates. The concentrates and filtrates were collected and their exact volume recorded. The concentrating factor was calculated as the volume ratio of the filtrate to concentrate. An average concentrating factor of 3.5, 3.7 and 4.2 for the 3 μm, 7 μm and 14 μm units, respectively, was found for tests using flow rates between 0.4 and 2 L/min. By substituting these values of R_{ref1} and R_{ref2} into equations (5) and (6), the number of μC units per refining level was obtained, considering that L1 and L2 should collect

concentrate volumes of < 200 mL from 10 L and 100 L samples. Thus, the filtration system showed in Fig. 22 was constructed with eight units to process 10 L of water. For 100 L samples, the system was constructed with ten units.

Oocyst and cyst recovery were tested with two separate apparatuses. The 3 μm unit L1 and 7 μm unit L2 were used for the oocyst recovery, while the 7 μm unit L1 and 14 μm unit L2 was tested for cysts. Fig. 23 shows the results for the recovery of oocysts and cysts spiked in 10 L river water at 10 organisms/L concentration, which is an acceptable detection limit criterion for evaluating environmental samples according to protozoa monitoring guidelines [105]. The highest recovery was achieved at a flow rate of 1.2 L/min. Therefore, this flow rate was used for further tests of reproducibility. Inspection of the multi-μC unit filtration system with a stereo-microscope revealed that the μC units did not suffer from significant particle adhesion. The turbine-blade profile of the micropillars in the CFR cell (Fig. 21) and the large filtration area of the multi-unit system may have enhanced clogging resistance [101].

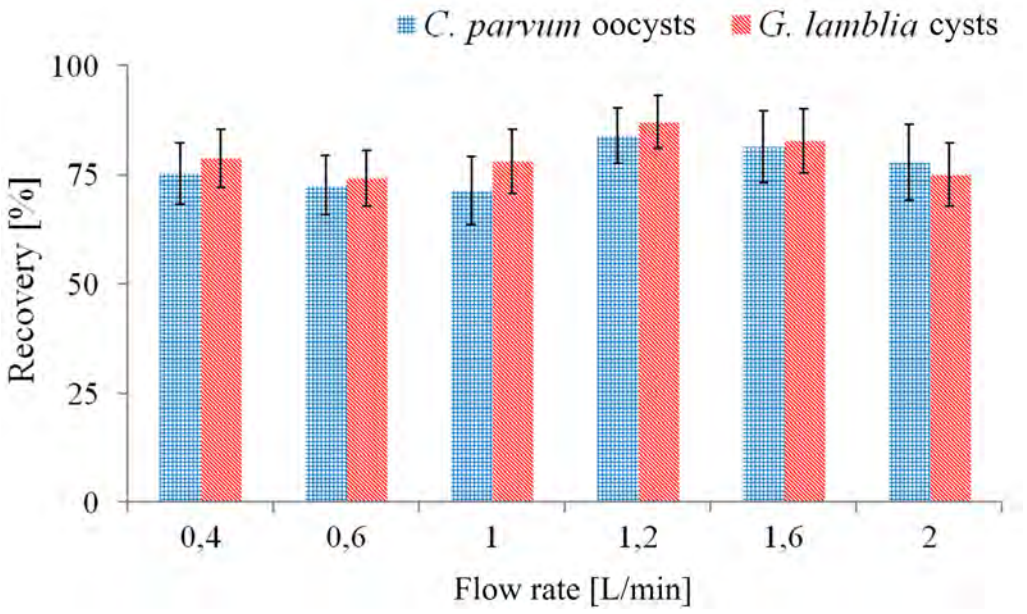

Fig. 23. Recovery of *C. parvum* oocysts and *G. lamblia* cysts from 10 L river water samples with the multi-μC unit filtration system. Detection of 10 organisms/L was conducted via IMS/IFM method.

The effect of the spiking dose and water volume was analysed in further reproducibility tests. Briefly, the results of these tests showed that protozoan recovery did not vary with spiking dose. According to six environmentally realistic oocyst and cyst concentrations (< 100 organisms/L), the mean recovery was 81.3% and 86.2% for *C. parvum* and *G. lamblia*, respectively. The separation of particulates in L1 from the target organisms

collected in L2 may have contributed to a decrease in the turbidity of the final L2 concentrate, thus enhancing the protozoan recovery [74]. Particulates above 7 μm and 14 μm in size could interfere with the recovery of *C. parvum* oocysts and *G. lamblia* cysts [106]. No significant difference in recovery efficiency was observed for 10 L and 100 L water samples.

2.3.2.2 Cascade-like particle separation Si filter

A drawback of the multi-unit filtration system described in *Section 2.3.2.1* is the use of a number of tubing connections between the μC units. A compact version of the particle refining system is then demonstrated by arranging multiple μC units into a cascade-like structure. This design allows multiplex separation of interfering water particulates from the target organisms. The developed cascade-like refining system was used as pre-filter for five conventionally used filters. The recovery of spiked *C. parvum* oocysts from 10 L of surface water was two- to three-fold higher when employing the pre-filter than when using the conventional filters alone. The cascade-like refining filter may be a feasible approach for improving filtration performance for large volume environmental water samples.

Design and experiments

The cascade-like arrangement of three μC units is shown in Fig. 24(a). The units are incorporated into a polycarbonate packaging device with the fluid channels for connecting the different units. The collection layer of one μC is connected to the active layer of the adjacent chip. Thus, when the main flow passes through the units, the water particulates separated in the active layer are collected in the concentrate flow of each μC, while non-separated particulates are guided into the filtrate flow between the units. Screwed holes are arranged in the packaging devices to serve as the inlet and outlet ports for connecting external tubing.

The μC of the upper refining unit (μC_1) has a gap that is larger than that of the lower refining unit. When a water sample flows into the cascade-like particle refining system, all the particulates larger than the gap of the upper unit are separated from the smaller ones that are collected and separated in the next refining unit. The target concentrate containing the protozoan organisms is collected in the refining unit placed at the bottom of the system (μC_3). To preconcentrate the *C. parvum* oocysts, the top and bottom units

incorporate the 10 μm and 3 μm gap μCs, respectively, while the middle unit contains the 7 μm gap concentrator. With this design, particulates larger than 7 μm and smaller than 3 μm in size can be separated prior to membrane filter processing.

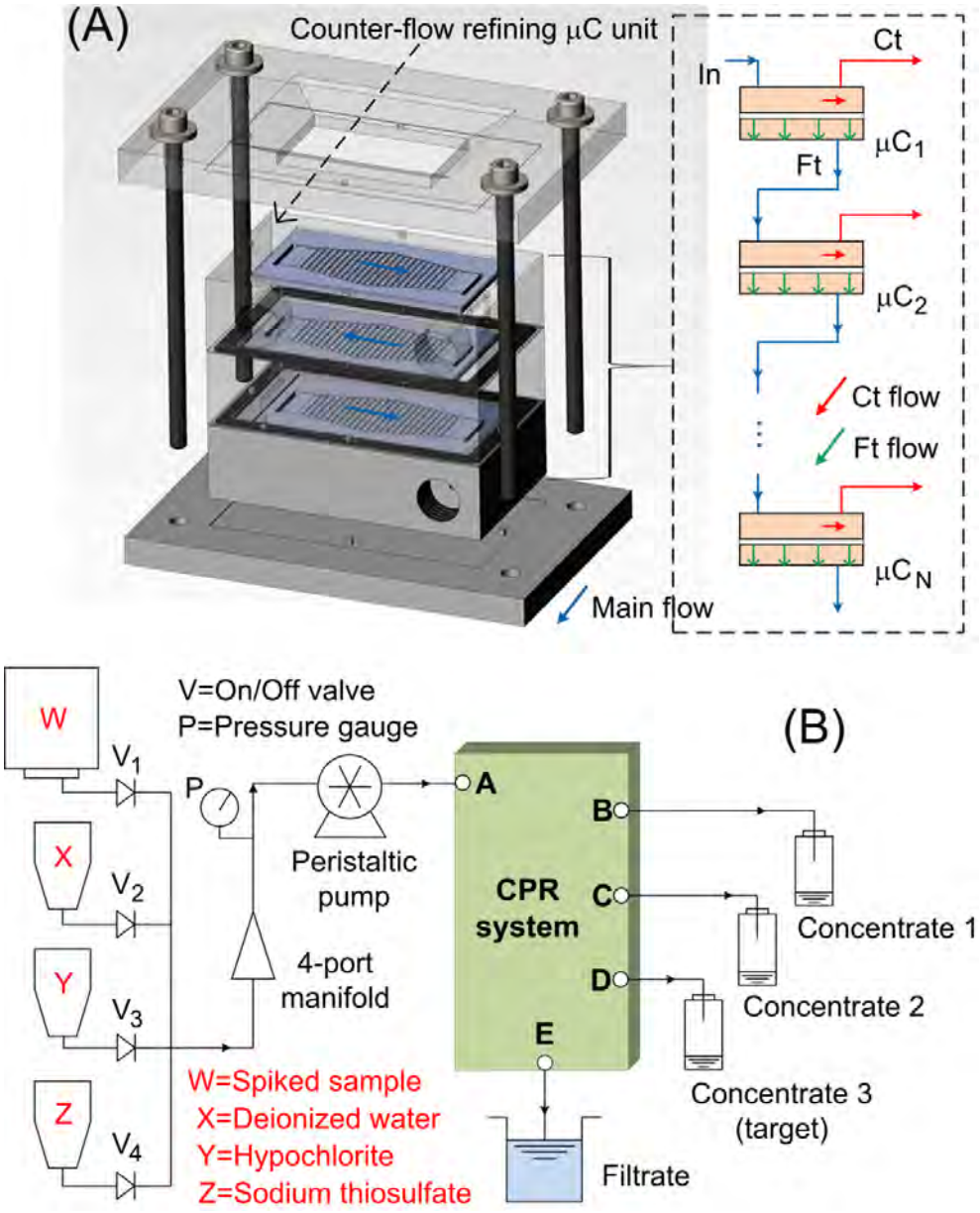

Fig. 24. (a) Cascade-like particle refining (CPR) system with incorporated three μC units (μC_1: 10 μm gap; μC_2: 7 μm gap; μC_3: 3 μm gap). (b) Procedure of cascade-like filtration for the pre-separation of water particulates and pre-concentration of protozoan organisms from 10 L water samples.

The design of the cascade-like filter integrates no valves or other fluid control components. It also provides an increased active area and decreased flow resistance for water filtration. Furthermore, a unique characteristic of the filter is that the number of μC units can be adjusted according to the turbidity of sample, which is useful because

high-turbidity water may require a large number of units while low-turbidity samples can be processed by fewer units. The concentrating ratio is characterized by

$$\frac{Q_{\mathrm{ctN}}}{Q_{\mathrm{in}}} = \prod_{n=1}^{N}\left(\frac{R_{n-1}}{R_n + 1}\right), \tag{7}$$

with $R_0 = 1$. In the expression, Q_{in} is the volumetric flow rate at the inlet of μC_1, Q_{ctN} is the volumetric flow at the concentrate outlet of the bottom μC, and R is the inherent concentrating factor of each separate μC.

Results and discussion

The 3, 7 and 10 μm gap μC units were preliminary tested with 10 L of river water without spiked *C. parvum* oocysts to determine the concentrating ratio R [see equation (7)] of each unit. The turbidity of the surface water was 15.3 nephelometric turbidity units (NTU) on average as measured by a commercial turbidimeter. The values of R obtained within the interval of 0.4-2 L/min were applied to equation (7), and the concentrating factor for the assembled three-unit refining system was estimated. The top, middle and bottom refining units were characterised by a concentrating factor of 5, 5.9 and 7.1, respectively for the filtration of 10 L samples.

Recovery performance was then analysed by testing the filter with 10-L river water samples spiked with 100 oocysts. Water filtration was conducted with the apparatus described in Fig. 24(b) with minor modifications. The concentrates were recirculated through the cascade-like filter until obtaining 100-200 mL. Recirculation was monitored by placing a flow meter after the filtrate outlet of the system. The water tested had an average turbidity of 32.5 NTU. The concentrates and filtrate were centrifuged at 1100 × g for 15 min prior to IMS/IFM analysis. Furthermore, between test runs of spiked water, non-spiked samples (10 L) were filtered, and the turbidity of the resulting concentrates and filtrate was measured. The recovery results shown in Fig. 25(a) revealed that the recovery rate was approximately 85% in the target concentrate (i.e., concentrate 3). Meanwhile, the percentage of the total number of oocysts lost in concentrate 1, concentrate 2 and filtrate did not exceed 12.3%. Moreover, the data shown in Fig. 25(b) indicate that the high oocyst recovery obtained in concentrate 3 was correlated to decreasing water turbidity. The turbidity measured for concentrate 1, concentrate 2 and filtrate demonstrated multiplex separation of particulates, and the results were in

agreement with those of Krometis *et al.* [106], who showed that the protozoan recovery was positively correlated to a reduction of particulates with diameters ranging from 2 to 30 μm.

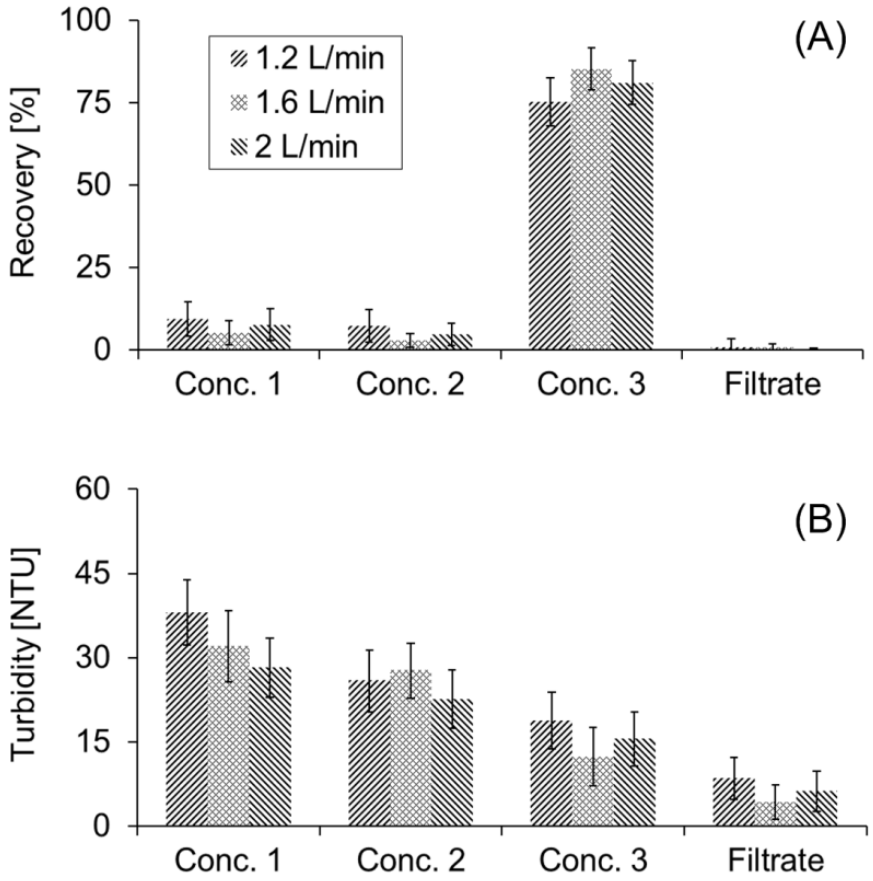

Fig. 25. (a) Recovery of *C. parvum* oocysts in the final concentrate 1 (Conc. 1), concentrate 2 (Conc. 2) and concentrate 3 (Conc. 3) and filtrate of the cascade-like particle refining system (see setup of Fig. 24) tested with river water samples. (b) Measurement of turbidity of the concentrates and filtrate after processing non-spiked samples.

After demonstrating recovery efficiency, the refining system was combined with compressed foam depth filters (Filta-Max), capsule filters (Envirochek standard and Envirochek HV), polycarbonate track-etched filters and multi(cellulose acetate—cellulose nitrate) filters. Two sets of experiments were then conducted: (1) spiked water samples were processed by the five filters using the cascade-like refining system as a pre-filter and (2) the conventional filters were tested without pre-filtration for comparison. Filter elution was performed according to the instructions of the manufacturer, and turbidity measurements were made for the filter eluates. Table 5 summarises the results of eluate turbidity and recovery efficiency for five filters using the refining system as a pre-filter. This data was compared with that obtained with the

five filters tested without pre-filtration. Consequently, the recovery efficiency of the Filta-Max depth filter, polycarbonate track-etched filter and multi(cellulose acetate—cellulose nitrate) filter increased nearly three-fold with the use of the refining pre-filter. In addition, a two-fold increase in recovery was achieved for the Envirochek standard capsule filter and Envirochek HV capsule filter by employing the pre-filter. Furthermore, sample pre-filtration led to decreased eluate turbidity, which might have been associated with increased oocyst recovery. This would be an important improvement for filtration because the methods widely used for protozoan recovery have been characterised by poor efficiencies when processing large-volume surface water samples [104, 108].

Conventional Filter	**Eluate turbidity (NTU)**	**Recovery efficiency (%)**
Filta-Max compressed foam filter	23.2	70.1
Envirochek standard capsule filter	34.5	50.4
Envirochek HV capsule filter	21.6	72.4
Polycarbonate track-etched filter	32.5	45.2
Multi(cellulose acetate—cellulose nitrate) filter	44.7	42.7

Table 5: Detection of *C. parvum* oocysts in spiked river water samples processed by five conventional filters with pre-filtration by the cascade-like particle refining system. Average values are shown for the eluate turbidity and recovery efficiency.

The pre-separation or refining of particulates reduced their accumulation and adhesion to the surface of the conventional filters. Hence, no clogging was encountered in the tested filters employing the refining pre-filter. Moreover, particulate pre-separation may have enhanced IMS and IFM performance, as high concentrations of particulates in water can greatly interfere with antibody specificity and binding [109].

3 Main conclusions and perspectives

This thesis aimed to develop cutting-edge strategies for the realisation of low-cost, high-sensitivity optical microfluidic biosensors. The development of a highly sensitive polymer photodetector for enhanced CL detection and its integration into polymer microfluidic chips was addressed in this work. Furthermore, a method for enhancing bio-analyte recovery from complex samples was also investigated. The performance and reliability of the developed microfluidic devices have been characterised systematically. The main conclusions are as follows:

- An organic photodetector constructed with the ITO/PEDOT:PSS/PCDTBT:$PC_{70}BM$/LiF/Al structure was exploited for microfluidic CL detection for the first time. The dark current and EQE parameters were critical for enhancing the CL detection sensitivity. Optimising the thickness of the PCDTBT:$PC_{70}BM$ photoactive layer and the PEDOT:PSS hole transport layer improved the OPD response to 425 nm light generated by CL reactions of HRP-luminol-H_2O_2. An EQE of over 60% and a background current of a few pA were obtained after OPD optimisation. Using the optimised OPD for the detection of clinically relevant protein analytes, the opto-microfluidic biosensor exhibited a linear response of over four orders of magnitude, with a detection limit of approximately tens of picograms per millilitre and a detection sensitivity of approximately hundreds of picograms per millilitre. This microfluidic biosensor concept advances the development of POC devices while retaining adequate sensitivity, cost, and compactness.
- A multiplexed microfluidic biosensor with multiple PCDTBT:$PC_{70}BM$ OPDs integrated into a hybrid polymer microfluidic chip was demonstrated for the first time. This biosensor is amenable to mass production. The dark current and responsivity were reproducible between different OPD pixels. The parallel detection of waterborne pathogens targeted in CL immunoassays was feasible.

Moreover, one parallel test could be performed in less than 35 min, and the multiplexed detection was extended to real water samples.

- A simple inexpensive opto-microfluidic device with enhanced sensitivity was developed by integrating a PCDTBT:$PC_{70}BM$ OPD and a hybrid microfluidic chip modified with AuNPs. The enhancing effect of AuNPs on CL led to a resolution of few picograms per millilitre for the detection of an environmentally relevant protein analyte. This resolution represents an improvement of ~200 times over previously reported CL sensors that employ other OPDs. Only a small decrease in photocurrent was observed after 15 days of tests without applying a protective encapsulation to the OPD due to the remarkable stability of the PCDTBT:$PC_{70}BM$ blend heterojunction.
- The thesis also addresses the recovery of bio-analytes from complex samples. The proposed particle refining systems are promising high-efficiency alternatives to currently used methods for the recovery of protozoan organisms from environmental water samples. The recovery efficiency for *C. parvum* and *G. lamblia* exceeded 80% employing a simple filtration procedure. Further, the ability of the refining system to pre-separate interfering water particulates from the target organisms allows significant improvement of the recovery performance for standard filters.

This work offers promising new approaches to realise high-efficiency sample preparation and high-sensitivity optical detection in low-cost microfluidic chips, which may have far-reaching implications for the design of future POC systems. The proposed setups are applicable to various bio-analyte types using different antibodies for the CL immunoassays and different gap sizes for the μC units.

Although the opto-microfluidic devices with integrated PCDTBT:$PC_{70}BM$ OPD were preliminarily challenged with a few samples of complex matrices, the comprehensive evaluation of the device utility in practical situations would require testing of a significant number of clinical trials. The potential uses of OPDs as integrated photodetectors in LOC devices are not limited to the PCDTBT:$PC_{70}BM$ OPDs. Other semiconducting polymers and blend heterojunction devices with outstanding stability and sensitivity to low light-level optical detection can be studied in future work. Furthermore, the background photocurrent that limits D^* of the OPDs can be further reduced by developing device structures with multi-layer blocking electrodes to

suppress the thermally generated dark current. The development of OPDs offering comparable D^* to the Si photodiode at a price comparable to that of the photoresistor would be a tremendous advance in optoelectronic detectors for LOCs. Another interesting direction for future research would be to develop a miniaturised electronic readout that is monolithically integrated with the OPD. This design would make the optoelectronic detection more practical. However, designing and fabricating on-chip electronics for ~pA current-level readout is not trivial, and it should be noted that a very sensitive Keithley SMU was used for the measurements conducted in this study. To address this challenge, different electrode configurations rather than the conventional diode architecture can be implemented to enhance the output photocurrent because ~μA current levels would be accessible for standard on-chip readouts. Moreover, fully autonomous opto-microfluidic devices could be realised by incorporating microstructures for on-chip reagent storage and passive fluid delivery.

The particle refining systems demonstrated in this doctoral work showed compatibility with standard optical detection of waterborne protozoa in real water samples. However, these systems are not limited to use with only IMS and IFM. Combination of the refining filters with optical detection technologies performed on microfluidic chips could be addressed in future research. The selectivity of the refining filters may be compromised in cases where multiple target organisms are similar in size. In this regard, the filters may be combined with high-selectivity DEP methods while retaining high organism recovery efficiency and non-clogging filtration of large volume water samples.

References

[1] P. Picotti, R. Aebersold, Selected reaction monitoring-based proteomics: workflows, potential, pitfalls and future directions, Nat. Methods 9 555-566 (2012).

[2] T. M. Straub and D. P. Chandler, Towards a unified system for detecting waterborne pathogens, J. Microbiol. Meth. 53 185-197 (2003).

[3] C. R. Taitt, J. P. Golden, Y. S. Shubin, L. C. Shriver-Lake, K. E. Sapsford, A. Rasooly, F. S. Ligler, A portable array biosensor for detecting multiple analytes in complex samples, Microbial Ecol. 47 175-185 (2004).

[4] J. E. Bandow, Comparison of protein enrichment strategies for proteome analysis of plasma, Proteomics 10 1416-1425 (2010).

[5] M. L. Y. Sin, K. E. Mach, P. K. Wong, J. C. Liao, Advances and challenges in biosensor-based diagnosis of infectious diseases, Expert Rev. Mol. Diagn. 14 225-244 (2014).

[6] U. Dharmasiri, M. A. Witek, A. A. Adams, J. K. Osiri, M. L. Hupert, T. S. Bianchi, S. A. Soper, Enrichment and detection of Escherichia coli O157:H7 from water samples using an antibody modified microfluidic chip, Anal. Chem. 82 2844-2849 (2010).

[7] H.-A. Keserue, H. P. Fuchslin, T. Egli, Rapid detection and enumeration of Giardia lamblia cysts in water samples by immunomagnetic separation and flow cytometric analysis, Appl. Environ. Microbiol. 77 5420-5427 (2011).

[8] K. R. Wigginton, P. J. Vikesland, Gold-coated polycarbonate membrane filter for pathogen concentration and SERS-based detection, Analyst 135 1320-1326 (2010).

[9] A. H. C. Ng, K. Choi, R. P. Luoma, J. M. Robinson, A. R. Wheeler, Digital microfluidic magnetic separation for particle-based immunoassays, Anal. Chem. 84 8805-8812 (2012).

[10] G. M. Whitesides, The origins and the future of microfluidics, Nature 442 368-373 (2006).

[11] J. T. Connelly and A. J. Baeumner, Biosensors for the detection of waterborne pathogens Anal. Bioanal. Chem. 402 117-127 (2012).

[12] A. Kaushik, A. Vasudev, S. K. Arya, S. K. Pasha, S. Bhansali, Recent advances in cortisol sensing technologies for point-of-care application, Biosens. Bioelectron. 53 499-512 (2014).

[13] C. D. Chin, V. Linder, S. K. Sia, Lab-on-a-chip devices for global health: past studies and future opportunities, Lab Chip 7 41-57 (2007).

[14] D. Mark, S. Haeberle, G. Roth, F. von Stetten, R. Zengerle, Microfluidic lab-on-a-chip platforms: requirements, characteristics and applications, Chem. Soc. Rev. 39 1153-1182 (2010).

[15] C. Rivet, H. Lee, A. Hirsch, S. Hamilton, H. Lu, Microfluidics for medical diagnostics and biosensors, Chem. Eng. Sci. 66 1490-1507 (2011).

[16] A. Ríos, M. Zougagh, M. Avila, Miniaturization through lab-on-a-chip: utopia or reality for routine laboratories? A review, Anal. Chim. Acta 740 1-11 (2012).

[17] C. D. Chin, V. Linder, S. K. Sia, Commercialization of microfluidic point-of-care diagnostic devices, Lab Chip 12 2118-2134 (2012).

[18] J. F. Rusling, C. V. Kumar, J. S. Gutkind, V. Patel, Measurement of biomarker proteins for point-of-care early detection and monitoring of cance, Analyst 135 2496-2511 (2010).

[19] V. Gubala, L. F. Harris, A. J. Ricco, M. X. Tan, D. E. Williams, Point of Care diagnostics: status and future, Anal. Chem. 82 487-515 (2012).

[20] P. Neužil, S. Giselbrecht, K. Länge, T. J. Huang, A. Manz, Revisiting lab-on-a-chip technology for drug discovery, Nat. Rev. Drug Discov. 11 620-632 (2012).

[21] K. B. Mogensen, H. Klank, J. P. Kutter, Recent developments in detection for microfluidic systems, Electrophoresis 25 3498-3512 (2004).

[22] J. Wang, Electrochemical biosensors: Towards point-of-care cancer diagnostics, Biosens. Bioelectron. 21 1887-1892 (2006).

[23] P. S. Waggoner, H. G. Craighead, Micro- and nanomechanical sensors for environmental, chemical, and biological detection, Lab Chip 7 1238-1255 (2007).

[24] S. Srivastava, Md. A. Ali, P. R. Solanki, P. M. Chavhan, M. K. Panday, A. Mulchandani, A. Srivastava, B. D. Malhotra, Mediator-free microfluidics biosensors based on titania-zirconia nanocomposite for urea detection, RSC Adv. 3 228-235 (2013).

[25] W. Dungchai, O. Chailapakul, C. S. Henry, Electrochemical detection for paper-based microfluidics, Anal. Chem. 81 5821-5826 (2009).

[26] J. Lu, S. Ge, L. Ge, M. Yan, J. Yu, Electrochemical DNA sensor based on three-dimensional folding paper device for specific and sensitive point-of-care testing, Electrochim. Acta 80 334-341 (2012).

[27] F. B. Myers, L. P. Lee, Innovations in optical microfluidic technologies for point-of-care diagnostics, Lab Chip 8 2015-2031 (2008).

[28] R. van den Hurk, S. Evoy, Deflection cantilever detection of interferon gamma, Sens. Act. B-Chem. 176 960-965 (2013).

[29] C. Ricciardi, G. Canavese, R. Castagna, I. Ferrante, A. Ricci, S. L. Marasso, L. Napione, F. Bussolino, Integration of microfluidic and cantilever technology for biosensing application in liquid environment, Biosens. Bioelectron. 26 1565-1570 (2010).

[30] R. R. Anderson, W. Hu, J. W. Noh, W. C. Dahlquist, S. J. Ness, T. M. Gustafson, D. C. Richards, S. Kim, B. A. Mazzeo, A. T. Woolley, G. P. Nordin, Transient deflection response in microcantilever array integrated with polydimethylsiloxane (PDMS) microfluidics, Lab Chip 11 2088-2096 (2011).

[31] X. Y. Z. Karsunke, R. Niessner, M. Seidel, Development of a multichannel flow-through chemiluminescence microarray chip for parallel calibration and detection of pathogenic bacteria, Anal. Bioanal. Chem. 395 1623-1630 (2009).

[32] A. M. Foudeh, T. F. Didar, T. Veres, M. Tabrizian, Microfluidic designs and techniques using lab-on-a-chip devices for pathogen detection for point-of-care diagnostics, Lab Chip 12 3249-3266 (2012).

[33] B. Kuswandi, Nuriman, J. Huskens, W. Verboom, Optical sensing systems for microfluidic devices: a review, Anal. Chim. Acta 601 141-155 (2007).

[34] F. S. Ligler, Perspective on optical biosensors and integrated sensor systems, Anal. Chem. 81 519-526 (2009).

[35] O. Gustafsson, K. B. Mogensen, P. D. Ohlsson, Y. Liu, S. C. Jacobson, J. P. Kutter, A electrochromatography chip with integrated waveguides for UV absorbance detection, J. Micromech. Microeng. 18 055021 (2008).

[36] S. K. Sia, V. Linder, B. A. Parviz, A. Siegel, G. M. Whitesides, An integrated approach to a portable and low-cost immunoassay for resource-poor settings, Angew. Chem. Int. Ed. 43 498-502 (2004).

[37] D. M. Vykoukal, G. P. Stone, P. R. C. Gascoyne, E. U. Alt, J. Vykoukal, Quantitative detection of bioassays with a low-cost image-sensor array for integrated microsystems, Angew. Chem. Int. Ed. 121 7785-7790 (2009).

[38] S. Wang, X. Zhao, I. Khimji, R. Akbas, W. Qiu, D. Edwards, D. W. Cramer, B. Ye, U. Demirci, Integration of cell phone imaging with microchip ELISA to detect ovarian cancer HE4 biomarker in urine at the point-of-care, Lab Chip 11 3411-3418 (2011).

[39] F. Yang, X.-c. Li, W. Zhang, J.-b. Pan, Z.-g. Chen, A facile light-emitting-diode induced fluorescence detector coupled to an integrated microfluidic device for microchip electrophoresis, Talanta 84 1099-1106 (2011).

[40] L. Shen, M. Ratterman, D. Klotzkin, I. Papautsky, A CMOS optical detection system for point-of-use luminescent oxygen sensing, Sens. Act. B-Chem. 155 430-435 (2011).

[41] N. Yildirim, F. Long, C. Gao, M. He, H. C. Shi, A. Z. Gu, Aptamer-based optical biosensor for rapid and sensitive detection of 17β-estradiol in water samples, Environ. Sci. Technol. 46 3288-3294 (2012).

[42] N. Ramalingam, Z. Rui, H.-B. Liu, C.-C. Dai, R. Kaushik, B. Ratnaharika, H.-Q. Gong, Real-time PCR-based microfluidic array chip for simultaneous detection of multiple waterborne pathogens, Sens. Act. B-Chem. 145 543-552 (2010).

[43] X. Zhao, T. Dong, Z. Yang, N. Pires, N. Hoivik, Compatible immune-NASBA LOC device for quantitative detection of waterborne pathogens: design and validation, Lab Chip 12 602-612 (2012).

[44] V. Charwat, M. Purtscher, S. F. Tedde, O. Hayden, P. Ertl, Standardization of microfluidic cell cultures using integrated organic photodiodes and electrode arrays, Lab Chip 13 785-797 (2013).

[45] A. Pais, A. Banerjee, D. Klotzkin, I. Papautsky, High-sensitivity, disposable lab-on-a-chip with thin-film organic electronics for fluorescence detection, Lab Chip 8 794-800 (2008).

[46] M. Miyake, H. Nakajima, A. Hemmi, M. Yahiro, C. Adachi, N. Soh, R. Ishimatsu, K. Nakano, K. Uchiyama, T. Imato, Performance of an organic photodiode as an optical detector and its application to fluorometric flow-immunoassay for IgA, Talanta 96 132-139 (2012).

[47] A. Banerjee, Y. Shuai, R. Dixit, I. Papautsky, D. Klotzkin, Concentration dependence of fluorescence signal in a microfluidic fluorescence detector, J. Lumin. 130 1095-1100 (2010).

[48] M. A. Cooper, Optical biosensors in drug discovery, Nat. Rev. Drug Discov. 1 515-528 (2002).

[49] A. M. Foudeh, J. T. Daoud, S. P. Faucher, T. Veres, M. Tabrizian, Sub-femtomole detection of 16s rDNA from legionella pneumophila using surface plasmon resonance imaging, Biosens. Bioelectron. 52 129-135 (2014).

[50] O. Krupin, H. Asiri, C. Wang, R. N. Tait, P. Berini, Biosensing using straight long-range surface plasmon waveguides, Opt. Express 21 698-709 (2013).

[51] E. Ouellet, C. Lausted, T. Lin, C. W. T. Wang, L. Hood, E. T. Lagally, Parallel microfluidic surface plasmon resonance imaging arrays, Lab Chip 10 581-588 (2010).

[52] K. M. Mayer and J. H. Hafner, Localized surface plasmon resonance sensors, Chem. Rev. 111 3828-3857 (2011).

[53] A. Ambrosi, F. Airò, A. Merkoçi, Enhanced gold nanoparticle based ELISA for a breast cancer biomarker, Anal. Chem. 82 1151-1156 (2010).

[54] N. M. M. Pires, T. Dong, U. Hanke, N. Hoivik, Integrated optical microfluidic biosensor using a polycarbazole photodetector for point-of-care detection of hormonal compounds, J. Biomed. Opt. 18 097001 (2013).

[55] M. Hao, Z. Ma, An ultrasensitive chemiluminescence biosensor for carcinoembryonic antigen based on autocatalytic enlargement of immunogold nanoprobes, Sensors 12 17320-17329 (2012).

[56] M. Yang, S. Sun, Y. Kostov, A. Rasooly, An automated point-of-care system for immunodetection of staphylococcal enterotoxin B, Anal. Biochem. 416 74-81 (2011).

[57] A. Roda, M. Mirasoli, L. S. Dolci, A. Buragina, F. Bonvicini, P. Simoni, M. Guardigli, Portable device based on chemiluminescence lensless imaging for personalized diagnostics through multiplex bioanalysis, Anal. Chem. 83 3178-3185 (2011).

[58] P. Novo, D. M. F. Prazeres, V. Chu, J. P. Conde, Microspot-based ELISA in microfluidics: chemiluminescence and colorimetry detection using integrated thin-film hydrogenated amorphous silicon photodiodes, Lab Chip 11 4063-4071 (2011).

[59] D. Caputo, G. de Cesare, L. S. Dolci, M. Mirasoli, A. Nascetti, A. Roda, R. Scipinotti, Microfluidic chip with integrated a-Si:H photodiodes for chemiluminescence-based bioassays, IEEE Sensors J. 13 2595-2602 (2013).

[60] J. R. Wojciechowski, L. C. Shriver-Lake, M. Y. Yamaguchi, E. Fureder, R. Pieler, M. Schamesberger, C. Winder, H. J. Prall, M. Sonnleitner, F.S. Ligler, Organic photodiodes for biosensor miniaturization, Anal. Chem. 81 3455-3461 (2009).

[61] R. Shinar, J. Shinar, Organic Electronics in Sensors and Biotechnology, McGraw-Hill, New York, 2009, ISBN 978-0-07-159676-3.

[62] X. Wang, M. Amatatongchai, D. Nacapricha, O. Hofmann, J. C. de Mello, D. D. C. Bradley, A. J. de Mello, Thin-film organic photodiodes for integrated on-chip chemiluminescence detection – application to antioxidant capacity screening, Sens. Act. B-Chem. 140 643-648 (2009).

[63] X. Wang, O. Hofmann, R. Das, E. M. Barrett, A. J. deMello, J. C. deMello, D. D. C. Bradley, Integrated thin-film polymer/fullerene photodetectors for on-chip microfluidic chemiluminescence detection, Lab Chip 7 58-63 (2007).

[64] H. A. Morales-Morales, G. Vidal, J. Olszewski, C. M. Rock, D. Dasgupta, K. H. Oshima, S. B. Smith, Optimization of reusable hollow-fiber ultrafilter for simultaneous concentration of enteric bacteria, protozoa, and viruses from water, Appl. Environ. Microbiol. 69 4098-4102 (2003).

[65] A. L. Polaczyk, J. Narayanan, T. L. Cromeans, D. Hahn, J. M. Roberts, J. E. Amburgey, V. R. Hill, Ultrafiltration-based techniques for rapid and simultaneous concentration of multiple microbe classes from 100-L tap water samples, J. Microbiol. Meth. 73 92-99 (2008).

[66] I-F. Cheng, C.-C. Lin, D.-Y. Lin, H.-C. Chang, A dielectrophoretic chip with a roughened metal surface for on-chip surface-enhanced Raman scattering analysis of bacteria, Biomicrofluidics 4 034104 (2010).

[67] F. Fabbri, S. Carloni, W. Zoli, P. Ulivi, G. Gallerani, P. Fici, E. Chiadini, A. Passardi, G. L. Frassineti, A. Ragazzini, D. Amadori, Detection and recovery of circulating colon cancer cells using a dielectrophoresis-based device: KRAS mutation status in pure CTCs, Cancer Lett. 335 225-231 (2013).

[68] S. Park, Y. Zhang, T.-H. Wang, S. Yang, Continuous dielectrophoretic bacterial separation and concentration from physiological media of high conductivity, Lab Chip 11 2893-2900 (2011).

[69] H. Bridle, M. Kersaudy-Kerhoas, B. Miller, D. Gavriilidou, F. Katzer, E. A. Innes, M. P. Y. Desmulliez, Detection of Cryptosporidium in miniaturised fluidic devices, Water Res. 46 1641-1661 (2012).

[70] D. S. Zarlenga, J. M. Trout, Concentrating, purifying, and detecting waterborne parasites, Vet. Parasitol. 126 195-217 (2004).

[71] U. Zuckerman, S. Tzipori, Portable continuous flow centrifugation and method 1623 for monitoring of waterborne protozoa from large volumes of various water matrices, J. Appl. Microbiol. 100 1220-1227 (2006).

[72] Wohlsen T, Bates J, Gray B, Katouli M. Evaluation of five membrane filtration methods for recovery of Cryptosporidium and Giardia isolates from water samples. Appl. Environ. Microbiol. 70 2318-2322 (2004).

[73] U. Dharmasiri, M. A. Witek, A. A. Adams, J. K. Osiri, M. L. Hupert, T. S. Bianchi, D. L. Roelke, S. A. Soper, Enrichment and detection of Escherichia coli O157:H7 from water samples using an antibody modified microfluidic chip, Anal. Chem. 82 2844-2849 (2010).

[74] M. E. Warkiani, L. Chen, C.-P. Lou, H.-B. Liu, R. Zhang, H.-Q. Gong, Capturing and recovering of Cryptosporidium parvum oocysts with polymeric microfabricated filter, J. Membrane Sci. 369 560-568 (2011).

[75] H. M. Ji, V. Samper, Y. Chen, C. K. Heng, T. M. Lim, L. Yobas, Silicon-based microfilters for whole blood cell separation, Biomed. Microdevices 10 251-257 (2008).

[76] R. C. Kuhn, K. H. Oshima, Evaluation and optimization of a reusable hollow fiber ultrafilter as a first step in concentrating Cryptosporidium parvum oocysts, Water Res. 35 2779-2783 (2001).

[77] T. Dong, Z. Yang, Q. Su, N. M. Tran, E. B. Egeland, F. Karlsen, Y. Zhang, M. J. Kapiris, H. Jakobsen, Integratable nonclogging microconcentrator based on counter-flow principle for continuous enrichment of CaSki cells sample, Microfluid. Nanofluid. 10 855-865 (2011).

[78] Y. Y. Feng, S. L. Ong, J. Y. Hu, S. F. Song, X. L. Tan, W. J. Ng, Effect of particles on the recovery of Cryptosporidium oocysts from source water samples of various turbidities, Appl. Environ. Microbiol. 69 1898-1903 (2003).

[79] J. Qiu, Y. Zhou, H. Chen, J.-M. Lin, Immunomagnetic separation and rapid detection of bacteria using bioluminescence and microfluidics, Talanta 79 787-795 (2009).

[80] United States Environmental Protection Agency, Method 1623: Cryptosporidium and Giardia in water by filtration/IMS/FA, EPA815-R-05–002, Office ofWater, United States Environmental Protection Agency, Washington D.C., USA, 2005.

[81] A. J. Heeger, Semiconducting polymers: the Third Generation, Chem. Soc. Rev. 39 2354-2371 (2010).

[82] S. H. Park, A. Roy, S. Beaupré, S. Cho, N. Coates, J. S. Moon, D. Moses, M. Leclerc, K. Lee, A. J. Heeger, Bulk heterojunction solar cells with internal quantum efficiency approaching 100%, Nat. Photonics 3 297-302 (2009).

[83] K. K. H. Chan, S. W. Tsang, H. K. H. Lee, F. So, S. K. So, Charge injection and transport studies of poly(2,7-carbazole) copolymer PCDTBT and their relationship to solar cell performance, Org. Electron. 13 850-855 (2012).

[84] E. Ouellet, C. W. T. Yang, T. Lin, L. L. Yang, E. T. Lagally, Novel carboxyl-amine bonding methods for poly(dimethylsiloxane)-based devices, Langmuir 26 11609-11614 (2010).

[85] B. Friedel, P. E. Keivanidis, T. J. K. Brenner, A. Abrusci, C. R. McNeill, R. H. Friend, N. C. Greenham, Effect of layer thickness and annealing of PEDOT:PSS layers in organic photodetectors, Macromolecules 42 6741-6747 (2009).

[86] B. V. Andersson, D. M. Huang, A. J. Moldé, O. Inganäs, An optical spacer is no panacea for light collection in organic solar cells, Appl. Phys. Lett. 94 043402 (2009).

[87] A. J. Moulé and K. Meerholz, Intensity-dependent photocurrent generation at the anode in bulk-heterojunction solar cells, Appl. Phys. B 92 209-218 (2008).

[88] T.-Y. Chu, S. Alem, P. G. Verly, S. Walkim, J. Lu, Y. Tao, S. Beaupré, M. Leclerc, F. Bélanger, D. Désilets, S. Rodman, D. Waller, R. Gaudiana, Highly efficient polycarbazole-based organic photovoltaic devices, Appl. Phys. Lett. 95 063304 (2009).

[89] C. Tlili, L. N. Cella, V. N. Myung, V. Shetty, A. Mulchandani, Single-walled carbon nanotube chemoresistive label-free immunosensor for salivary stress biomarkers, Analyst 135 2637-2642 (2010).

[90] S. K. Arya, G. Chornokur, M. Venugopal, S. Bhansali, Antibody functionalized interdigitated μ-electrode (IDμE) based impedimetric cortisol bionsensor, Analyst 135 1941-1946 (2010).

[91] R. C. Stevens, S. D. Soelberg, S. Near, C.E. Furlong, Detection of cortisol in saliva with a flow-filtered, portable surface plasmon resonance biosensor system, Anal. Chem. 80 6747-6751 (2008).

[92] A. Wolter, R. Niessner, M. Seidel, Detection of Escherichia coli O157:H7, Salmonella typhimurium, and Legionella pneumophila in water using a flow-through chemiluminescence microarray readout system, Anal. Chem. 80, 5854-5863 (2008).

[93] V. Sunkara, D.-K. Park, H. Hwang, R. Chantiwas, S. A. Soper, Y.-K. Cho, Simple room temperature bonding of thermoplastics and poly(dimethylsiloxane), Lab Chip, 11 962-965 (2011).

[94] B. Arredondo, B. Romero, J. M. S. Pena, A. Fernández-Pacheco, E. Alonso, R. Vergaz, C. de Dios, Visible light communication system using an organic bulk heterojunction photodetector, Sensors 13 12266-12276 (2013).

[95] M. Yang, Y. Kostov, H. A. Bruck, A. Rasooly, Gold nanoparticle-based enhanced chemiluminescence immunosensor for detection of Staphyloccocal Enterotoxin B (SEB) in food, Int. J. Food Microbiol. 133 265-171 (2009).

[96] H. Kanamori, F. Takada, Y. Sasaki, M. Yamanaka, and T. Yasuda, Development of a blood testing device based on localized surface plasmon resonance, Proceedings of 17th International Conference on Miniaturized Systems for Chemistry and Life Sciences (MicroTAS), 2013, 542-544.

[97] X. Gong, M. Tong, Y. Xia, W. Cai, J. S. Moon, Y. Cao, G. Yu, C.-L. Shieh, B. Nilsson, A. J. Heeger, High-detectivity polymer photodetectors with spectral response from 300 nm to 1450 nm, Science 325 1665-1667 (2009).

[98] G. Lu, B. Cheng, H. Shen, Z. Chen, G. Yang, C. A. Marquette, L. J. Blum, O. Tillement, S. Roux, G. Ledoux, A. Deschamps, P. Perriat, Influence of the nanoscale structure of gold thin films upon peroxidase-induced chemiluminescence, App. Phys. Lett. 88 023903 (2006).

[99] R. Ishimatsu, A. Naruse, R. Liu, K. Nakano, M. Yahiro, C. Adachi, An organic thin film photodiode as a portable photodetector for the detection of alkylphenol polyethoxylates by a flow fluorescence-immunoassay on magnetic microbeads in a microchannel, Talanta 117 139-145 (2013).

[100] N. Yanagisawa, D. Dutta, Enhancement in the sensitivity of microfluidic enzyme-linked immunosorbent assays through analyte preconcentration, Anal. Chem. 84, 7029-7036 (2012).

[101] S. Zheng, J. Liu, Y. Tai, Streamline-based microfluidic devices for erythrocytes and leukocytes separation, J. Microelectromech. Syst. 17, 1029-1038 (2008).

[102] R. C. Kuhn, K. H. Oshima, Hollow-fiber ultrafiltration of Cryptosporidium parvum oocysts from a wide variety of 10-l surface water samples, Can. J. Microbiol. 48, 542-549 (2002).

[103] Y. Y. Feng, S. L. Ong, J. Y. Hu, L. F. Song, X. L. Tan, W. J. Ng, Effect of particles on the recovery of Cryptosporidium oocysts from source water samples of various turbidities, App. Environ. Microbiol. 69, 1898-1903 (2003).

[104] J. Hu, Y. Feng, S. L. Ong, W. J. Ng, L. Song, X. Tan, X. Chu, Improvement of recoveries for the determination of protozoa Cryptosporidium and Giardia in water using method 1623, J. Microbiol. Meth. 68, 321-325 (2004).

[105]] J. A. Moss, R. A. Snyder, Pathogenic protozoa, in C. Hagedorn, A. R. Blanch, V. J. Harwood, Microbial source tracking: methods, applications, and case studies, Springer, New York, 2011, ISBN 978-1-4419-9385-4.

[106] L.-A. H. Krometis, G. W. Characklis, M. D. Sobsey, Identification of particle size classes inhibiting protozoan recovery from surface water samples via U.S. Environmental Protection Agency Method 1623, Appl. Environ. Microbiol. 75 6619-6621 (2009).

[107] H. D. A. Lindquist, S. Harris, S. Lucas, M. Hartzel, D. Riner, P. Rochele, R. DeLeon, Using ultrafiltration to concentrate and detect Bacillus anthracis, Bacillus atrophaeus subspecies globigii, and Cryptosporidium parvum in 100-liter water samples, J. Microbiol. Meth. 70 484-492 (2007).

[108] C. L. DiGiorgio, D. A. Gonzalez, C. C. Huitt, Cryptosporidium and Giardia recoveries in natural waters by using Environmental Protection Agency Method 1623, Appl. Environ. Microbiol. 68 5952-5955 (2002).

[109] R. M. Hoffman, D. M. Wolk, S. K. Spencer, M. A. Borchardt, Development of a method for the detection of waterborne microsporidia, J. Microbiol. Meth. 70 312-318 (2007).

Papers not available in this file due to publisher's restrictions:

I:
Pires, N. M. M., Dong, T., Hanke, U., & Hoivik, N. (2013). Integrated optical microfluidic biosensor using a polycarbazole photodetector for point-of-care detection of hormonal compounds. *Journal of Biomedical Optics, 18*(9), 097001,1-097001,8. doi: 10.1117/1.JBO.18.9.097001

II:
Pires, N. M. M., & Dong, T. (2014). Measurement of salivary cortisol by a chemiluminescent organic-based immunosensor. *Bio-Medical Materials and Engineering, 24*(1), 15-20. doi: 10.3233/BME-130778

III:
Pires, N. M. M., & Tao, D. (2013). Multiplexed detection of waterborne pathogens with an array of microfluidic integrated high-sensitivity organic photodiodes. *Biomedical Circuits and Systems Conference (BioCAS), 2013 IEEE*, 105-108. doi: 10.1109/BioCAS.2013.6679650

IV:
Pires, N.M.M., & Dong, T. (2013). Microfluidic biosensor array with integrated poly(2,7-carbazole)/fullerene-based photodiodes for rapid multiplexed detection of pathogens. *Sensors, 13*(12), 15898-15911.

V:
Pires, N.M.M., & Dong, T. (2014). Ultrasensitive opto-microfluidic immunosensor integrating gold nanoparticle–enhanced chemiluminescence and highly stable organic photodetector. *Journal of Biomedical Optics, 19*(3), 030504-1-030504-3. doi: 10.1117/1.JBO.19.3.030504

VI:
Pires, N.M.M., & Dong, T. (2013). Recovery of Cryptosporidium and Giardia organisms from surface water by counter-flow refining microfiltration. *Environmental Technology (United Kingdom), 34*(17), 2541-2551. doi: 10.1080/09593330.2013.777126